An Airborne Study of Microwave Surface Sensing and Boundary Layer Heat and Moisture Fluxes for Project FIFE

Third Semiannual (Year 1.5) Status Report

Robert D. Kelly
Principal Investigator

1 July 1988 - 31 December 1988

Department of Atmospheric Science
University of Wyoming
P.O. Box 3038
Laramie, Wyoming 82071-3038

Grant NAG 5-913

1 Introduction

This document is the third semiannual status report describing the University of Wyoming participation in project FIFE, under NASA Grant NAG 5-913.

The reader is referred to the first and second semiannual status reports for this grant for descriptions of University of Wyoming participation in the field operations of 1987. The present report is concerned with continuing analysis of data collected in the field.

2 Instrumentation, analysis methods

Most of the instrument calibration effort has concentrated on interpretation and use of the high-rate water vapor measurements with the University of Wyoming Lyman-alpha device. In addition, fluxes of water vapor have been corrected for sensible heat flux, and, by committee decision, all the high-rate (10 Hz for the Wyoming King Air) data have been filtered before the flux calculations. All these techniques are discussed below:

Lyman-alpha calibration:

For each flight the Lyman-alpha data (10 Hz) are calibrated against the Cambridge dew-point hygrometer (1 Hz), by using data from the take-off sounding. The reasoning here is that the takeoff sounding (held to 500 fpm rate-of-climb specifically for the calibration) covers the widest range of humidity conditions of any sequence of the flight. For each takeoff sounding, then, the Lyman-alpha data, averaged to 1 Hz, are matched to the dew-point data with a second-order least-squares fit. The resulting quadratic equation is then used in all subsequent analyses to convert the Lyman-alpha voltages to vapor densities for that specific flight. An alternative method that has been suggested is to use the range of fluctuation for the same two devices from

horizontal passes to establish the calibration function. However, since the Lyman-alpha data are only used in the flux calculations, i.e., only the fluctuations and not the absolute values are used, this method is thought unnecessary.

Correction of vapor flux for heat flux

Following Webb et al. (1980), the vertical fluxes of water vapor and latent heat are corrected for sensible heat flux. The origin of this correction stems from the fact that in the eddy correlation method of calculating vertical fluxes of "trace" gases, the mean vertical velocity is removed before the calculations. However, since in conditions of positive vertical sensible heat flux, rising parcels will be less dense than corresponding sinking parcels, continuity (mass conservation) dictates that a small, but positive vertical velocity will exist. Webb et al. (1980) use the sensible heat flux to deduce this vertical velocity, and apply it as a correction to the vapor and latent heat fluxes. The form used with the King Air data is

$$F_{v,corr} = (1 + \mu\sigma)\left\{\overline{w'\rho'} + \frac{\bar{\rho}}{\bar{T}}(\overline{w'T'})\right\}$$

In this expression μ is the ratio of molecular weight for dry air to molecular weight for water, σ is the ratio of vapor density to dry air density, w′ is the vertical velocity fluctuation, ρ is the vapor density, and T′ is the temperature fluctuation. For the FIFE fluxes, corrections ranged up to 10% with this method.

Lyman-alpha time lag

Because the Lyman-alpha air sample is drawn from internal "plumbing" in the King Air, there is a time-lag of about 0.3 sec for the Lyman-alpha readings in comparison with the other,

externally mounted instruments, such as the gust and temperature probes. For this reason, all correlations that involve Lyman-alpha variables (vapor density, mixing ratio, etc.) are computed with a 0.3 sec lag.

Filtering of high-rate data

By decision of the ABL FIFE committee, all the high-rate data on the three aircraft involved in FIFE were filtered with a third-order, high-pass recursive filter prior to calculation of the eddy correlation fluxes. This approach was chosen over that of detrending (removing linear trends) in order to allow removal of non-linear, long-wave fluctuations in the data for individual, horizontal flight legs. The filter used on the King Air data was derived from the maximally-flat approximation of Budak (1974), transformed with the pole-zero technique of Jacquot (1981). The transformation uses a ripple of 1.0 dB and a cutoff frequency corresponding to a wavelength of 5 km ($f_{cutoff} = V/5km$, where V is the true airspeed). At an average airspeed of 85 m s^{-1} the cutoff frequency is 0.017 Hz. (It is also worth noting, here, that such a small cutoff frequency, given a sampling rate of 10 Hz and the corresponding Nyquist limit of 5 Hz, pushes the performance of this filter or any other high-pass filter to estreme limits.) In its final form the filtered value of each variable in a time series is a function of the three previous filtered values and the three previous unfiltered values:

$$O_k = K'(I_k - 3I_{k-1} + 3I_{k-2} - I_{k-3}) - JO_{k-1} - KO_{k-2} - LO_{k-3}$$

Here O's are the filtered values and I's are the unfiltered values at positions k (present position) through k-3 (0.3 sec prior to present position) in the time series. The constants J, K, and L are determined from the original approximation and the transformation.

3 Flux profiles and surface fluxes

3.1 Introduction

The primary aircraft flight pattern used in FIFE was a series of horizontal (constant pressure altitude) passes at various positions and at various levels over the FIFE experimental area, which was approximately 15 by 15 km. Various schemes were used to combine such passes for different types of measurements, especially in attempts to remove the effects of time changes during flight patterns which lasted from about 1 to more than 2 hours. The most successful pattern for this purpose we will refer to here as "time-centered," as conceived by Ray Desjardins. A time-centered flight pattern designed to measure vertical profiles of fluxes and other pass-averaged values is illustrated in Fig. 1. **Linear** changes in pass-averaged values can be removed since the averages for each pair of corresponding levels correspond to the same central point in time. Non-linear changes, of course, are not removed in the averaging process. A more complex time-centered pattern was designed and used for budget measurements. It is described in detail in section 5, below.

Since the philosophy of flight design evolved along with results and experience during the field experiment, not all the vertical flux profile measurements were taken with time-centered flights. Of the cases discussed below, 20 August and 7 and 8 October were based on time-centered flight sequences. The others (15 and 17 August, and 11 October) were not.

The locations of the horizontal flight legs used for all the measurements described in sections to follow are sketched in Fig. 2, along with the end-point notation used in the remainder

of the text. The center point in this figure is the intersection of Interstate 70 and Kansas highway 177, at the southeast corner of the Konza Prairie Preserve.

As mentioned above, the vertical fluxes were calculated with the eddy-correlation method, so that the sensible and latent heat fluxes for each horizontal flight leg are, respectively,

$$F_H = \rho C_p \overline{w'\theta'}$$

and

$$F_L = \rho L \overline{w'\rho'}$$

where C_p is the specific heat for moist air, ρ is the vapor density, θ is the potential temperature, and L is the latent heat of evaporation. The primes denote fluctuation, or perturbation values, after removal of the "means" with the third-order filter described above.

Each flight analysis includes values of sensible and latent heat fluxes measured at the FIFE surface sites. For each case, average surface values were calculated, simply as unweighted arithmetic means of all the stations during the time of the flux-profile portion of the aircraft flight. In general, surface values were archived at 0.5-hr intervals, so the surface means may include 2 to 4 values for each of about 17 sites. Data from station 26 were rejected form this analysis (early fall 1988) since it appeared the sensible and latent heat values were reversed (and reversed in sign, as well) and were generally far from agreement with the other stations. The locations of the surface sites are shown in Fig. 3, along with the locations of the aircraft passes used in the flux profiles.

3.2 Daily cases

In each case discussed below, the aircraft and surface data have been combined in one figure, plotting sensible and latent heats against average height above the surface. For the aircraft data, the range bars show the minimum-to-maximum range of values for the individual, pass-averaged fluxes used to calculate each height-averaged flux. For the surface fluxes, the average and two range bars are shown. The range bars drawn with thick lines extend over the mean±standard deviation range, while those drawn with thin lines extend over the minimum-to-maximum range of values.

Vertical flux profiles for 11 August are shown in Fig. 4, for flight data from 1718-1817 GMT, at three levels between the points FNW and FNE (an east-west line at 39°05.3′ N latitude. The 1712 GMT FIFE radiosonde shows an inversion height of about 1150 m agl, with a well-mixed layer below that level. The highest point reached on the aircraft flux profile was about 460 m agl, less than half the inversion height. For both F_H and F_L the decrease with height was nearly linear, with F_L greater than F_H by about a factor of 2. A linear projection of F_H to the surface would correspond to a value between F and F-f. of the values actually measured. (F is the mean sensible or latent heat flux; f is the standard deviation.) A linear projection of F_L to the surface would correspond to a value between F+f and the maximum of the values actually measured.

Vertical flux profiles for 15 August are shown in Fig. 5, for flight data from 1633-1804 GMT, at four levels between the points FNW and FNE (an east-west line at 39°05.3′ N latitude. The 1705 GMT FIFE radiosonde shows an inversion height of about 900 m agl, with most of the boundary layer thermally stable below that level. The highest point reached on the aircraft flux profile was about 460 m agl, about half the inversion

height. For the lowest three points of both the F_H and F_L profiles the decrease with height was nearly linear, with F_L greater than F_H by about a factor of 2. A linear projection of F_H to the surface would correspond to a value near the average of the values actually measured. A linear projection of F_L to the surface would correspond to a value between the miminum and F-f of the values actually measured.

Vertical flux profiles for 17 August are shown in Fig. 6, for flight data from 1723-1807 GMT at three levels between the points FNW and FNE (an east-west line at 39°05.3′ N latitude), and for flight data from 1815-1847 GMT for three levels between the points FN and FS (a north-south line at 96°33.0′ W longitude). The 1724 GMT FIFE radiosonde shows a stable increase of about 3 K over the first 1000 agl. The highest point reached on the aircraft flux profile was about 460 m agl. Both of the F_H profiles were nearly linear, while both the F_L profiles were distinctly non-linear, with F_L greater than F_H by about a factor of 3. In a general sense both F_H and F_L were nearly constant with height. A linear projection of F_H to the surface would correspond to a value between the minimum and F-f of the values actually measured. A rough projection of F_L to the surface would likewise correspond to a value between the miminum and F-f of the values actually measured.

Two profiles were derived from the 20 August data, both from time-centered sequences of flight legs (Fig. 7.). The profile at the north end of the study area contains three levels between the points FW0 and FE0 (1756-1833 GMT, 39°06.3′ N), while that at the south end of the study area contains three levels between FW6 and FE6, collected in two sets of passes (1718-1750 and 1853-1922 GMT, 38°59.2′ N). Thus the south-end profile spans a greater block of time than the north-end profile. The 1700 GMT

FIFE radiosonde shows a very stable boundary layer, with potential temperature increasing about 7 K in the first 1000 m agl. The highest points on the aircraft profiles are about 300 m agl. The F_H and F_L profiles at both locations are approximately linear, with F_L greater than F_H by about a factor of 3 at the lowest level. A projection of F_H to the surface would correspond to a value between F-f and F of the values actually measured, while a projection of F_L to the surface would correspond to a value less than the minimum of those actually measured.

Two separate flights were used on 7 October. Flux profiles for the first flight (Fig. 8) were derived from data at three levels between points FW2 and FE2 (39°03.3′ N), for 1701-1818 GMT. The 1747 GMT FIFE radiosonde showed an inversion at about 650 m agl. The highest flight level in the aircraft profiles was 270 m agl, less than half the height of the inversion. F_L was small for this period, being less than 30 Wm^{-2} at all levels. F_H decreased nearly linearly with height, and was about 7X F_H at the lowest levels. A projection of F_H to the surface would correspond to the minimum of the values actually measured, while a projection of F_L to the surface would correspond to a value between the minimum and F-f for those actually measured.

The second flight on 7 October used the same three levels and flight path as the first, for the period 2007-2115 GMT (Fig. 9). The 2107 FIFE radiosonde showed a well-mixed layer extending to about 650 m agl, with a stable layer from there to 1400 m and above. The highest flight level, then, was less than half the height of the mixed layer. Once again, F_H values in the aircraft profile were all less than 30 Wm^{-2}. F_L values decreased only slightly with height, and were about 5X F_H at the lowest level. A projection of F_H to the surface would corre-

spond to a value between the minimum and F-f for those actually measured, while a projection of F_L to the surface would fall below the minimum of the values actually measured.

Two profiles were derived from the 8 October data, both from time-centered sequences of flight legs. The data are presented in two figures. Fig. 10 includes the north- and south-end profiles, with only the average values at each level, as well as a profile formed from the average of all the data. Fig. 11 contains only the all-pass average profile, with minimum-to-maximum value ranges for each level.

The profile at the north end of the study area (Fig. 10) contains three levels between the points FNW and FNE (1843-1926 GMT, 39°05.3′ N), while that at the south end of the study area contains the same three levels between FW6 and FE6, collected in two sets of passes (1811-1833 and 1938-1959 GMT, 38°59.2′ N). Thus the south-end profile spans a greater block of time than the north-end profile. The 1826 GMT FIFE radiosonde shows a well-mixed boundary layer, capped by an inversion at about 920 m agl (see also Fig. 25). The highest points on the aircraft profiles are about 730 m agl. The F_H and F_L profiles at both locations are approximately linear, with F_L greater than F_H at the three lowest levels. Note that both profiles become negative at about the same height (600-700 m agl, about 2/3 the BL depth). Projections of F_H to the surface would correspond to values below the actual minimum for the south profile and between F-f and F for north profile. Projections of F_L to the surface would correspond to values between the minimum and F-f for both the north and south profiles.

Flux profiles for the flight on 11 October (Fig. 12) were derived from data at five levels between points FW2 and FE2 (39°03.3′ N), for 1701-1818 GMT. The 1826 GMT FIFE radiosonde showed a well-mixed boundary layer, capped by an inversion at

about 1050 m agl. The highest flight level in the aircraft profiles was 790 m agl. F_L was small for this period, being less than 20 $W m^{-2}$ at all levels except 670 m (perhaps an anomolous value?). F_H decreased nearly linearly with height, and was about 10X F_H at the lowest levels. A projection of F_H to the surface would fall below the minimum of the values actually measured, while a projection of F_L to the surface would correspond to about F-f for those actually measured.

General trends from the individual cases are best segregated according to season, since the weather and plant conditions of August 1987 were quite different from those of October. This general discussion occupies the following section.

3.3 Seasonal trends

The limiting values for the pass-average fluxes, for 11, 15, 17, and 20 August, are shown in Fig. 13, to illustrate the August flux environment. In all cases F_H was less than F_L, and in all cases F_H decreased monotonically with height. In one case the aircraft passes extended high enough in the BL to measure negative F_H values. Projections of F_H profiles to the surface were always at the "low end" of the range of surface values. F_H was always less than 150 $W m^{-2}$ for the lowest-level aircraft data; the surface **averages** ranged from 125 to 240 $W m^{-2}$. For projections of F_L to the surface the results are more "scattered." The projected values were usually at the low end of the range of surface values, but the projected values overlapped the surface averages. F_L for the lowest-level aircraft data was 180-350 $W m^{-2}$, while the surface averages ranged from 290 to 420 $W m^{-2}$.

Since the experimental period in August contained several intense rainfall episodes, a rough analysis was performed to see if day-to-day fluctuations in surface and aircraft flux values

for the 4 aircraft analysis days, had any correlation with the rainfall data. Fig. 14 shows the lowest-level aircraft and average surface values of F_H and F_L for each of those four dates, along with the daily average rainfall for FIFE, for 7-21 August. No obvious correlation is noted. Further analysis (hopefully the surface flux group has already done this) should include daily, if not hourly, surface flux values for every day in the period.

The range of aircraft-measured flux values for 7 (two flights), 8, and 11 October are shown in profile form in Fig. 15. In contrast to August, F_L was now much above zero for all these dates, ranging from 0 to 70 $W m^{-2}$ at the lowest flight levels. Surface averages, in agreement, ranged from 50-80 $W m^{-2}$. F_H, on the other hand, was 150-280 $W m^{-2}$ at the lowest flight levels, and decreased with height in all cases. Surface average F_H ranged from 230 to 370 $W m^{-2}$. Daily average rainfall and daily flux values for these October cases are plotted in Fig. 16, primarily for comparison with Fig. 14.

Finally, to contrast August and October, one can examine the overall ranges indicated in Figs. 13 and 15. Whereas latent heat fluxes dominated at all levels in August, they had become nearly zero at all levels by October. This is not surprising, since by October the surface vegetation was in senescence (?), and weather during the experimental period included almost no rainfall. Values of sensible heat flux increased at all levels from August to October, but even so never reached the levels of latent heat flux seen in August. Analysis of this increase and the limited values reached will be interesting to the project as a whole, since it must include a fairly complex picture of changing available solar energy (including the effects of decreasing atmospheric turbidity and decreasing atmospheric humidity), changing plant activity, and changing albedo, all

affecting the surface radiation and flux budget differently for IR, visible, and uv wavelengths. In order of increasing flux magnitude, then, we would list October F_L, August F_H, October F_H, and August F_L.

4 Gridded stack analysis (flux cross-section)

A first attempt has been made at gridded flux cross-section analysis for two of the FIFE flights (15 August and 7 October). In the first section below evidence is given that the statistics of such short-path analyses are questionable. In the second section the results are shown anyway, at least to allow comparison with the corresponding horizontal grid analysis of the Twin Otter data for the same dates.

4.1 Statistical basis (or nonbasis!)

To attempt construction of 2-D vertical cross-sections of fluxes over the FIFE site, the horizontal paths used in the profile analysis described above were each divided into four equal sections. Since the original paths comprised about 2.5 to 3 min of data, the subdivided, shorter sections comprise only about .6 to .75 min (36 to 45 sec, or 360 to 400 data points for the 10-Hz data).

To see the effects of reducing the averaging time on the flux values, two passes were examined in detail: 170851-171147 GMT, 1700 ft msl on 15 August, and 181112-181419 GMT, 1600 ft msl on 8 October. Three sets of time-reduced values have been generated. In set A the central time of the averaging period is held fixed, while the averaging period itself is reduced from the full pass to about 40 sec in 10-sec increments. In other words, the geographic point corresponding to each of the averages for set A is the geographic center of the original flight path. In set B the beginning time of the averaging period is held fixed, while the averaging period is reduced from the full

pass to about 40 sec in 10-sec increments. Set C is the same as B, except the end time is held fixed while the averaging period is reduced. Both the passes used in this analysis proceeded from west-to-east, so that for sets B and C the geographic center of the averaging period moves from the original center toward the west end of the pass ("west-justified", set B) or toward the east end ("east-justified," set C).

Figs. 17-19 show the results of this analysis for the pass on 15 August. Fig. 17 contains the F_H and F_L values for set A (central time fixed). The right-most values of F_H and F_L are full-pass values (about 1800 data points). Moving to the left corresponds to decreasing the averaging period, with a corresponding decrease in the number of data points. The resulting variation extends to about ±18% for both F_H and F_L.

Data from the west-justified set (B) are shown in the same format in Fig. 18. In this case both F_H and F_L increase as the averaging period is decreased, up to about 150% of the original values in both cases. For the east-justified set (C) drastic decreases in both F_H and F_L are noted, to about 45% of the original values.

For sets A, B, and C the shortest averaging period used was about 40 sec (400 points), corresponding to the length of the subdivided passes proposed for constructing the flux cross sections. Even in the case with the geographic center fixed (set A) the variation would seem large enough to obscure our ability to see the "real" segment-to-segment variation for the subdivided passes. In any case, a few examples of the results of such subdivision are presented below.

4.2 Discussion

Figs. 20 and 21 show contoured cross-sections (looking north at a west-east oriented plane) of sensible heat flux for two

profiles on 15 August. In each figure the "x"s indicate the center points of each of the four segments of the original flight paths, at four levels. The contour intervals are 20 Wm^{-2}. Near the surface the highest values are just to the west of center for both profiles (above 120 Wm^{-2} for the first profile, and above 100 Wm^{-2} for the second). At all higher levels, however, the pattern of relative high and low values looks nearly reversed from the first to the second cross-section. The obvious question here is whether this reversal is real, or whether it is an artifact of shortening the averaging period for the flux calculations. Since the point-to-point variation in F_H along a particular level (especially the two nearest to the surface) is not much more than 20%, and since a 4-to-1 reduction in averaging period could cause changes of about the same relative magnitude, the reality of the time and space variation implied in Figs. 20 and 21 is very questionable.

Similar, contoured cross-sections of sensible heat flux are shown in Figs. 22 and 23 for each of the two flights on 7 October. Again, the near-surface relative maximum appears to stay in the same location, while the relative maxima and minima at higher levels do not.

5 Budget analysis, 8 October 1987

5.1 General comments

Boundary layer development and conditions on 8 October were nearly "textbook" in general and in detail. Fig. 24 shows the evolution of the potential temperature profile with time over the FIFE site, based on 8 radiosondes from 1343 to 2207 GMT. As indicated, the boundary layer was well-mixed and capped by a strong inversion throughout this period, with boundary layer depth increasing steadily from about 200 m at 1343 GMT to about

1700 m by 2207 GMT. The flux-measurement portion of the aircraft operations on that day was 1811-1959 GMT. Profiles of water vapor mixing ratio, potential temperature, and wind speed and direction near the beginning of the flux measurement period, at 1826 GMT, are plotted in Fig. 25. Over the mixed-layer depth indicated by near-constant potential temperature (up to about 950 m agl), mixing ratio decreased slightly with height, while wind speed and direction were nearly constant (10-15 m s^{-1} from about 150°). Above the mixed layer the wind speed increased with height, while the wind direction changed to a southwesterly direction. Thus, the boundary layer was well-mixed in temperature and momentum during the period of flux/budget measurements.

5.2 Method and results

The flight design used for budget analysis on 8 October was a time-centered pattern, illustrated schematically in Fig. 26. Constant-altitude passes at four different levels were flown at the south and north ends of the FIFE area, starting and ending at the lowest pass level on the south end. By ordering the passes bottom to top at the south end, top to bottom then bottom to top at the north end, and top to bottom at the south end, averages of corresponding pass values at the south end and at the north end will all have the same "central" time. Likewise, averages for all passes at a given level will correspond to the same central time (identical to the central time for the north-end and south-end averages). Again, this design can only remove linear changes in various parameters with time.

Starting with the expanded (to include turbulence terms) heat conservation equation for the boundary layer, using Reynolds averaging for terms with perturbation quantities and assuming continuity, one finds for a dry boundary layer (Stull, 1988):

$$\frac{\partial \bar{\theta}}{\partial t} + \bar{u}\frac{\partial \bar{\theta}}{\partial x} + \bar{v}\frac{\partial \bar{\theta}}{\partial y} + \bar{w}\frac{\partial \bar{\theta}}{\partial z} = -\frac{1}{\bar{\rho} C_p}\frac{\partial \bar{Q}}{\partial z} - \partial\frac{\overline{w'\theta'}}{\partial z}$$

Most of the terms in this equation have been defined previously. The orientation of the positive x and y axes is eastward and northward, respectively, in this application. In the following discussion the individual terms will be referred to in numerical order, from left to right.

Term 1 was evaluated using averages of potential temperature at the south end of the site, since the elapsed times for those passes were the largest of any of the corresponding pass pairs. The average $\partial\bar{\theta}/\partial t$ was determined for each of the four levels, then these four values were averaged to find term 1 as 0.000398 Ks^{-1}.

As part of the routine data analysis, linear trends (i.e., the slopes ofleast-squares fits for first order equations) were determined for all of the high-rate variables. Since all the flight legs were oriented west-east and east-west, these trends give excellent estimates of west-east gradients, such as those needed to evaluate term 2. In this case, with one estimate of $\partial\bar{\theta}/\partial x$ for each pass, four values were averaged for an estimate at each of the four levels. These level-averages were then multiplied by the corresponding level-average u, and the resulting products averaged for an estimate of term 2 as 0.000026 Ks^{-1}.

The south-north gradient in term 3 was estimated at each level by finding the level-average potential temperatures separately for the north and south ends, dividing the difference between these averages by the north-south separation (10.98 km), and multiplying the resulting gradient times the level-average v (four values of v averaged per level). The resulting four products were averaged to estimate term 3 as 0.000068 Ks^{-1}.

To find term 4 continuity was assumed, and the average vertical velocity was computed as

$$\overline{w} = -\sum\left(\frac{\overline{\Delta u}}{\Delta x} + \frac{\overline{\Delta v}}{\Delta y}\right)\Delta z$$

The west-east gradient was estimated by averaging the linear trends for each level (see discussion of term 2), while the south-north gradient was found from level-average differences (see discussion of term 3). For the lowest level, Δz was taken as the average aircraft height agl. The resulting w was 0.007 m s^{-1}. The vertical gradient of potential temperature, estimated from level-average values, was about 10^{-4} K m^{-1}, giving term 4 as 0.0000007 Ks^{-1}. Term 4, then, may be ignored compared to the other terms.

For the remainder of the discussion, term 5 will be referred to as the residual, R, since the radiative flux divergence was not measured from the aircraft. As a residual, then, R may be due to the radiative processes, as well as to an accumulation of errors from the other terms.

Finally, term 6 is the slope of the least-squares linear fit to the four level-average values of $w'\theta'$ (each of which is the average of four pass values) plotted against height (Fig. 27). This slope, or term 6, is -0.000255 Ks^{-1}.

Combining all the above estimates leaves a residual, R, of 0.000237 Ks^{-1}. This is undoubtedly too large to be accounted for by radiative flux divergence, since it corresponds to warming at about 0.8 K h^{-1}. **Maximum** radiative flux divergence cooling rates, in nocturnal boundary layers, have been estimated from several model calculations as less than -0.4 K h^{-1} (Garrat and Brost 1981, Andre and Mahrt 1982, Stull 1983, Cerni and Parish 1984, Carlson and Stull 1986, and Turton and Brown 1987).

5.3 Internal consistency

Further examination of the heat budget data for 8 October should include an estimate of the entrainment flux of sensible heat through the capping inversion, to see how well it compares with the eddy-correlation measurements of sensible heat flux near the top of the mixed layer. The entrainment flux is given as $-\bar{\rho} C_p w_e \Delta\theta$, and the entrainment speed is calculated as

$$w_e = \frac{\partial z_i}{\partial t} - \bar{w}$$

where z_i is the inversion base height. The entrainment speed was estimated in two different ways for 8 October, while the average updraft was taken as 0.007 m s^{-1} (see discussion of term 4, above).

In the first instance, the rate of rise for the inversion was estimated by the Twin Otter crew as 0.0246 ms^{-1} and the change in potential temperature across the inversion as 4 K, giving w_e=0.0176 ms^{-1} and the entrainment flux as -74 Wm^{-2}.

The second estimate was taken from the FIFE radiosonde data (see Fig. 24), where the rate of rise of the inversion was 0.0446 ms^{-1} (least-squares fit to radiosonde values) and the change in potential temperature was about 5 K. These give w_e=0.0376 and an entrainment flux of -198 Wm^{-2}.

If one extrapolates the profile shown in Fig. 27 to an inversion height of 1090 m (corresponding to the mid-point of the aircraft measurements), the estimated sensible heat flux is -110 Wm^{-2}. This value lies in between the two, independent estimates given above. At the least it demonstrates a qualitative consistency in the data from various sources.

A second, and final look at the data consistency has already been mentioned in section 3, where extrapolations of the aircraft flux profiles were compared with averages and ranges for values measured at the surface sites. For 8 October, linear extrapolation of the aircraft sensible heat flux profile to the surface gives an estimate of 199 $W m^{-2}$. For the surface values collected during the same time period, the average was 303, standard deviation 48, minimum 202 and maximum 385 $W m^{-2}$. In other words, the extrapolated value matches the **minimum** surface measurement.

6 Plans for continuing analysis

Plans for continuation and completion of the above analyses include the following:

-- Combining the heat and moisture budget analyses from the Wyoming aircraft with those for the Canadian Twin Otter, in a joint publication (in progress as of this writing).

-- Continued comparison of the aircraft and surface flux data, in cooperation with the other aircraft group(s) and the surface flux group.

-- Use of conservative parameter analyses to estimate Bowen ratio profiles and variations at aircraft flight levels, and to compare these values with those measured at the surface. Again, this will be done in cooperation with the other aircraft investigators and with the surface flux investigators.

7 References

Budak, A., 1974: **Passive and Active Network Analysis and Synthesis.** Houghton Mifflin Co., Boston, 733 pp.

Jacquot, R. G., 1981: **Modern Digital Control Systems.** Marcel Dekker, Inc., New York, 355 pp.

Webb, E. K., G. I. Pearman, and R. Leuning, 1980: Correction of flux measurements for density effects due to heat and water vapour transfer. **Quart. J. Roy. Meteor. Soc., 106,** 85-100.

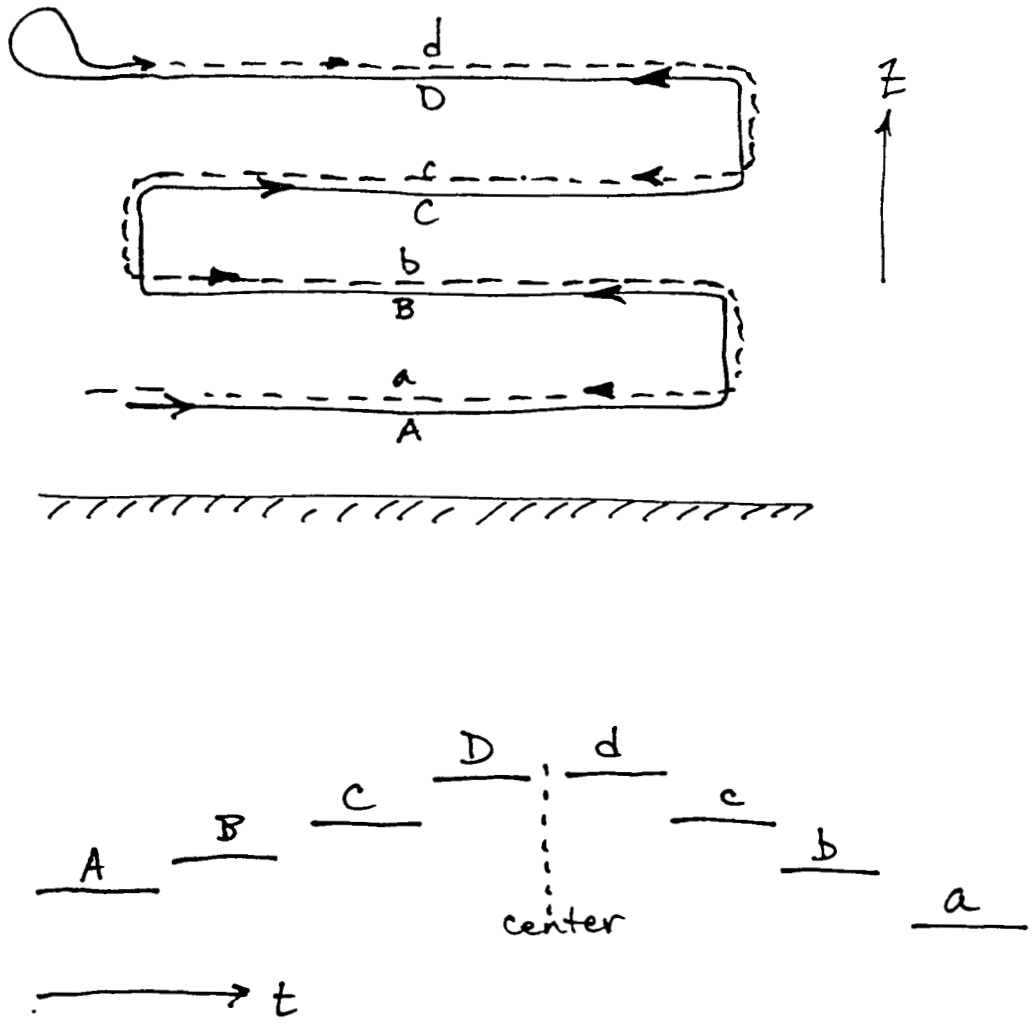

Fig. 1. Time-centered flight pattern used to measure vertical profiles of various parameters, including fluxes, in FIFE.

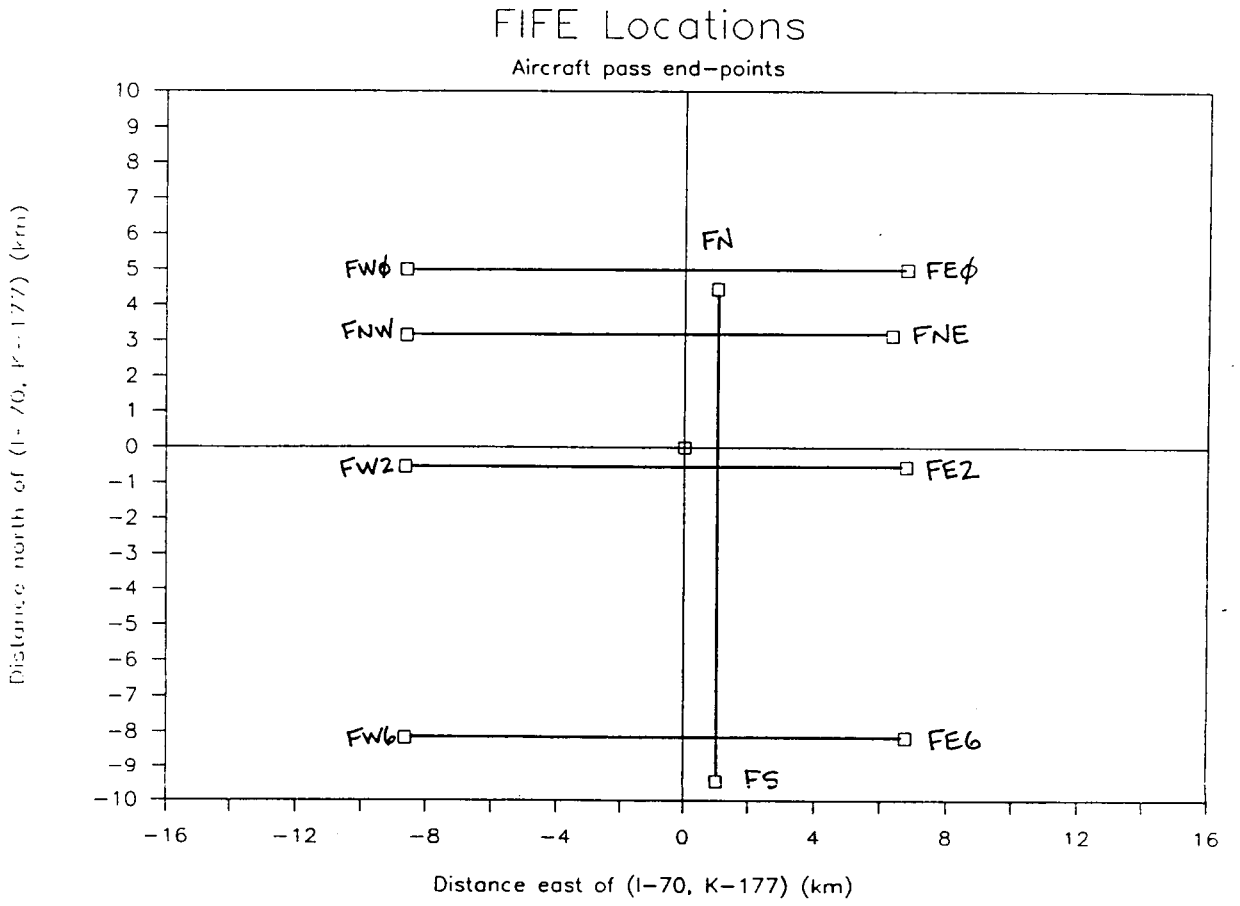

Fig. 2. Aircraft flight paths and reference points used in 1987 flux and budget analyses in FIFE. The origin of the (x,y) coordinates in this plot is the intersection of Interstate highway 70 and Kansas highway 177.

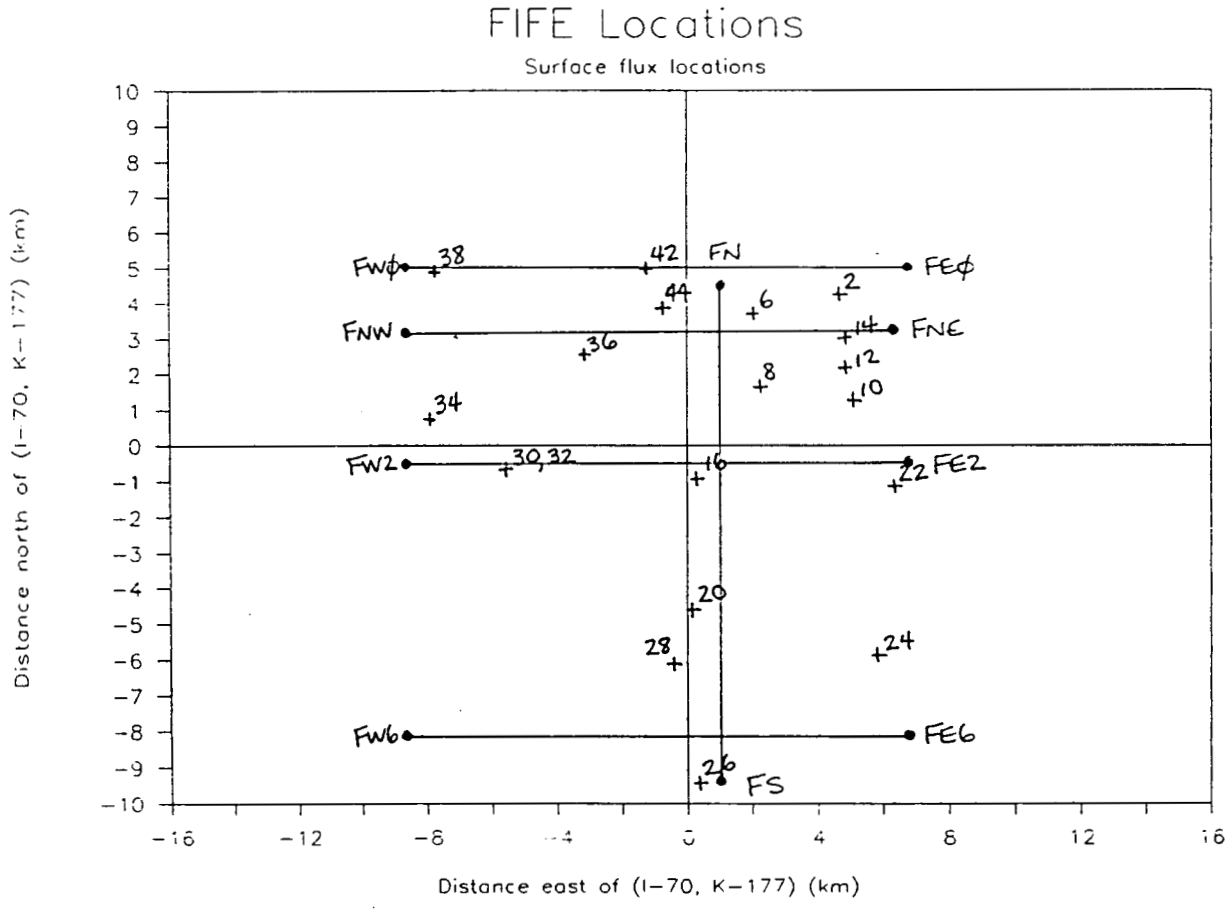

Fig. 3. Same as Fig. 2, but also including the locations and numbers of the surface flux measurement stations.

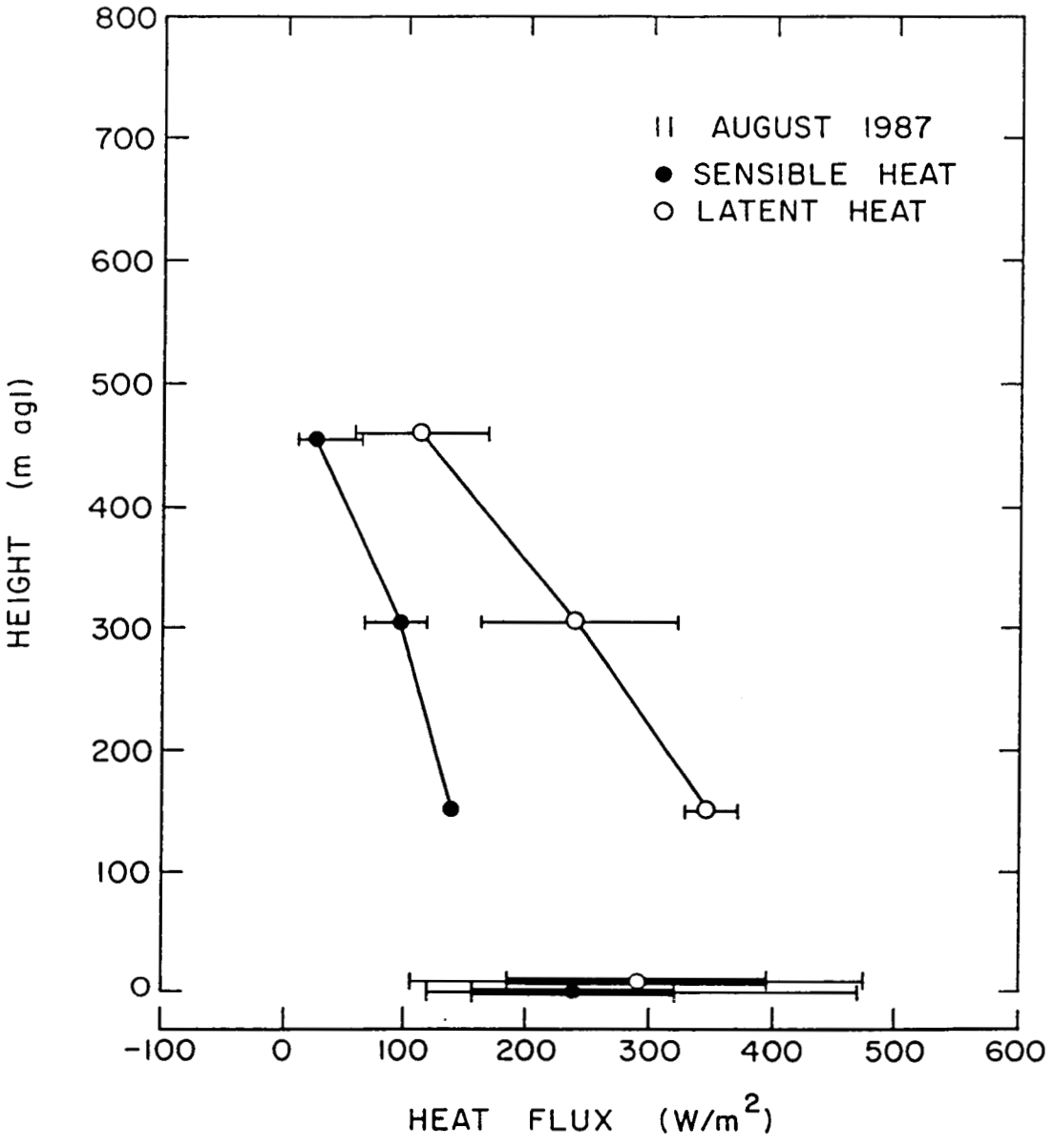

Fig. 4. Vertical profiles of sensible and latent heat fluxes for 11 August 1987, as calculated from data collected by the Wyomign King Air aircraft, and values of latent and sensible heat fluxes measured by the FIFE surface flux stations. See text for explanation of range bars on all the measurements.

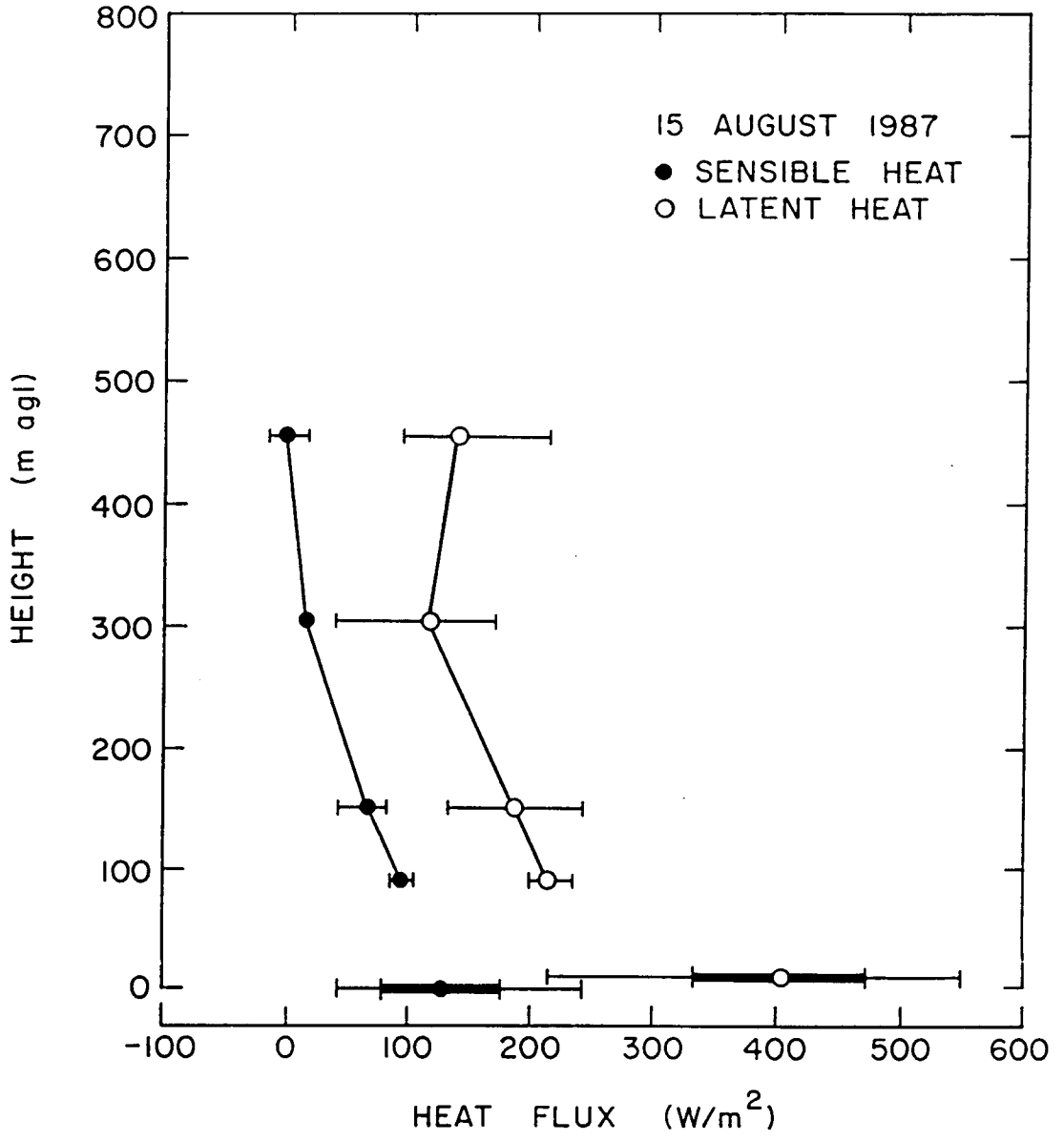

Fig. 5. Same as Fig. 4, for 15 August 1987.

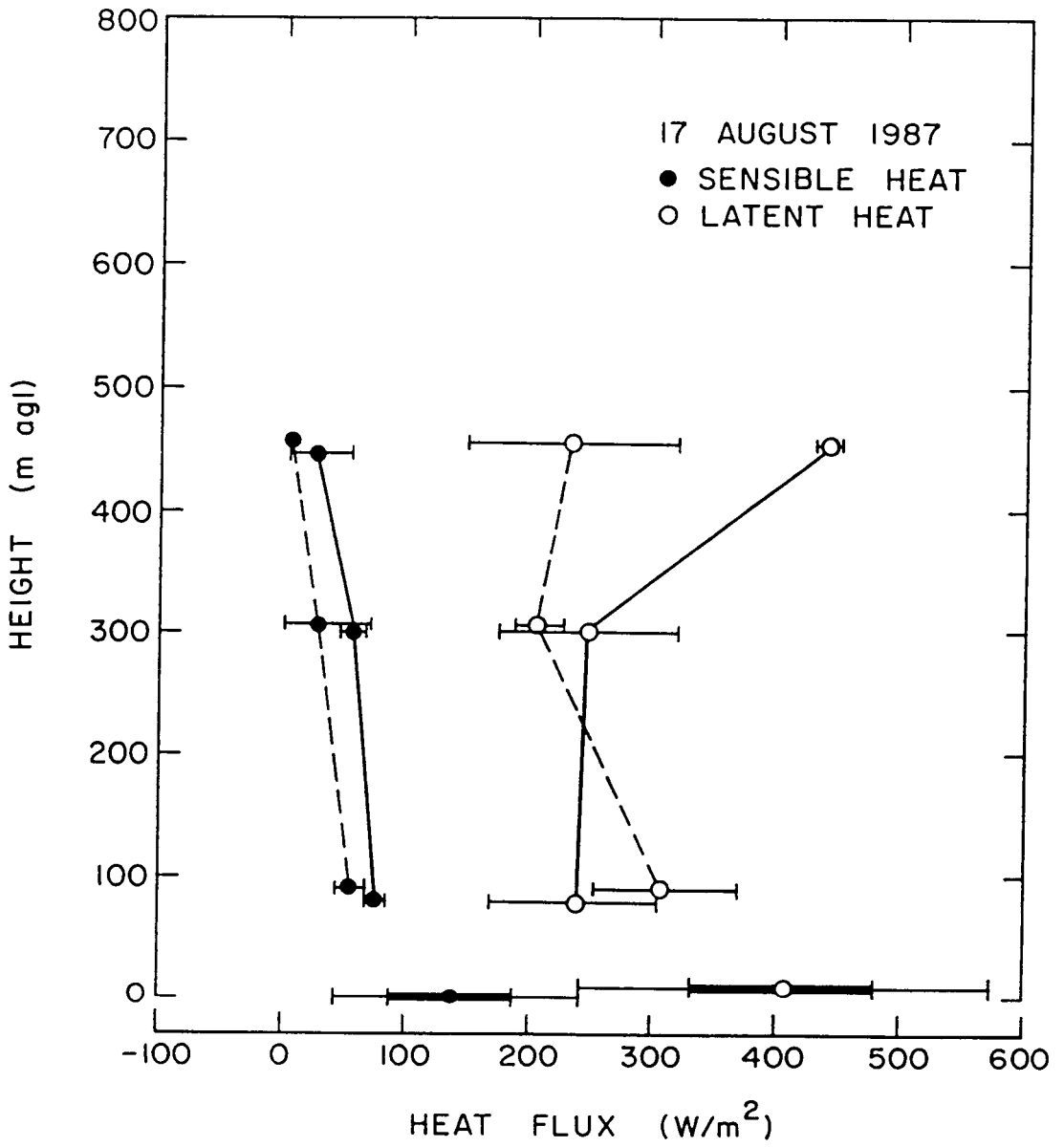

Fig. 6. Same as Fig. 4, for 17 August 1987.

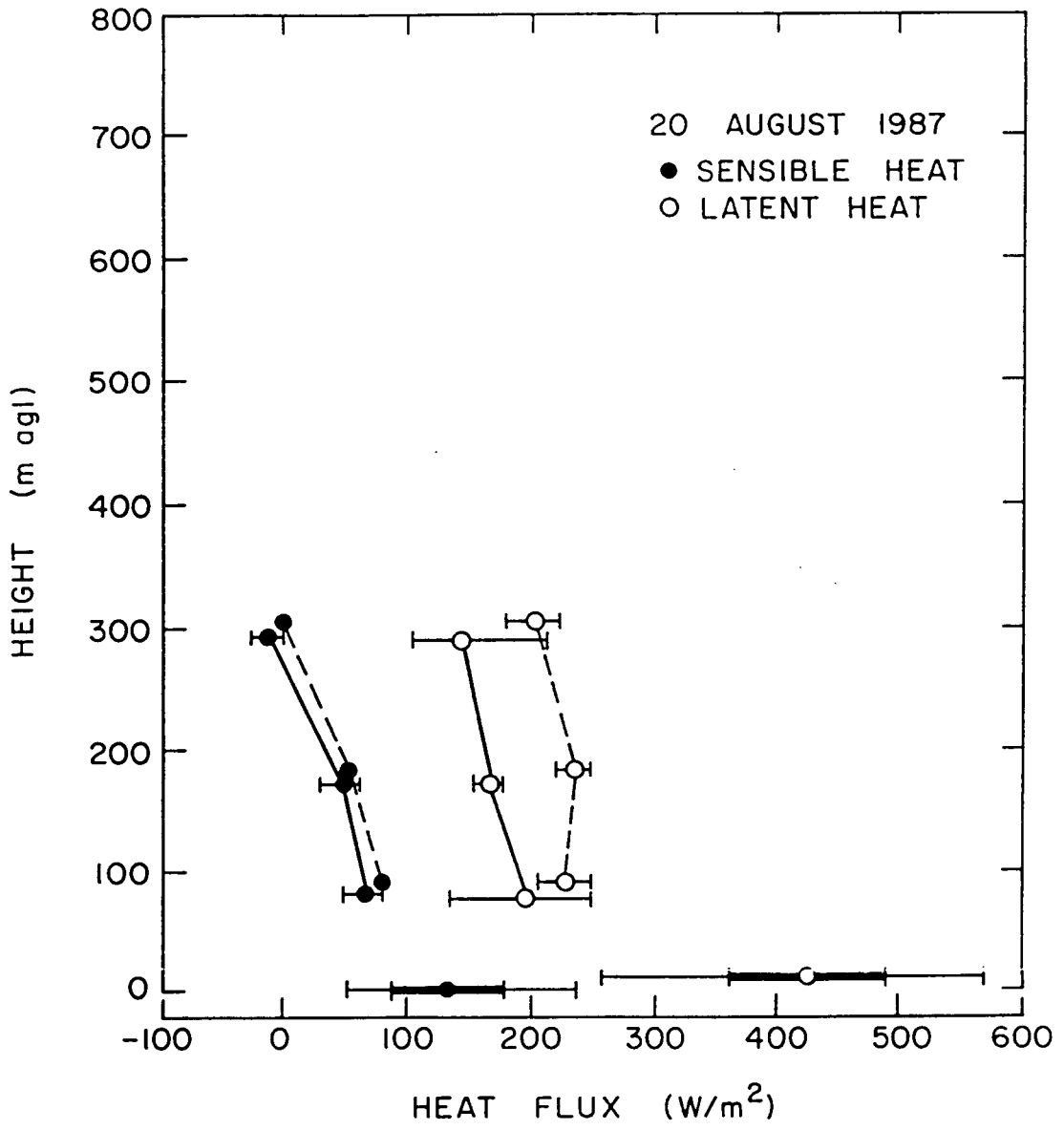

Fig. 7. Same as Fig. 4, for 20 August 1987.

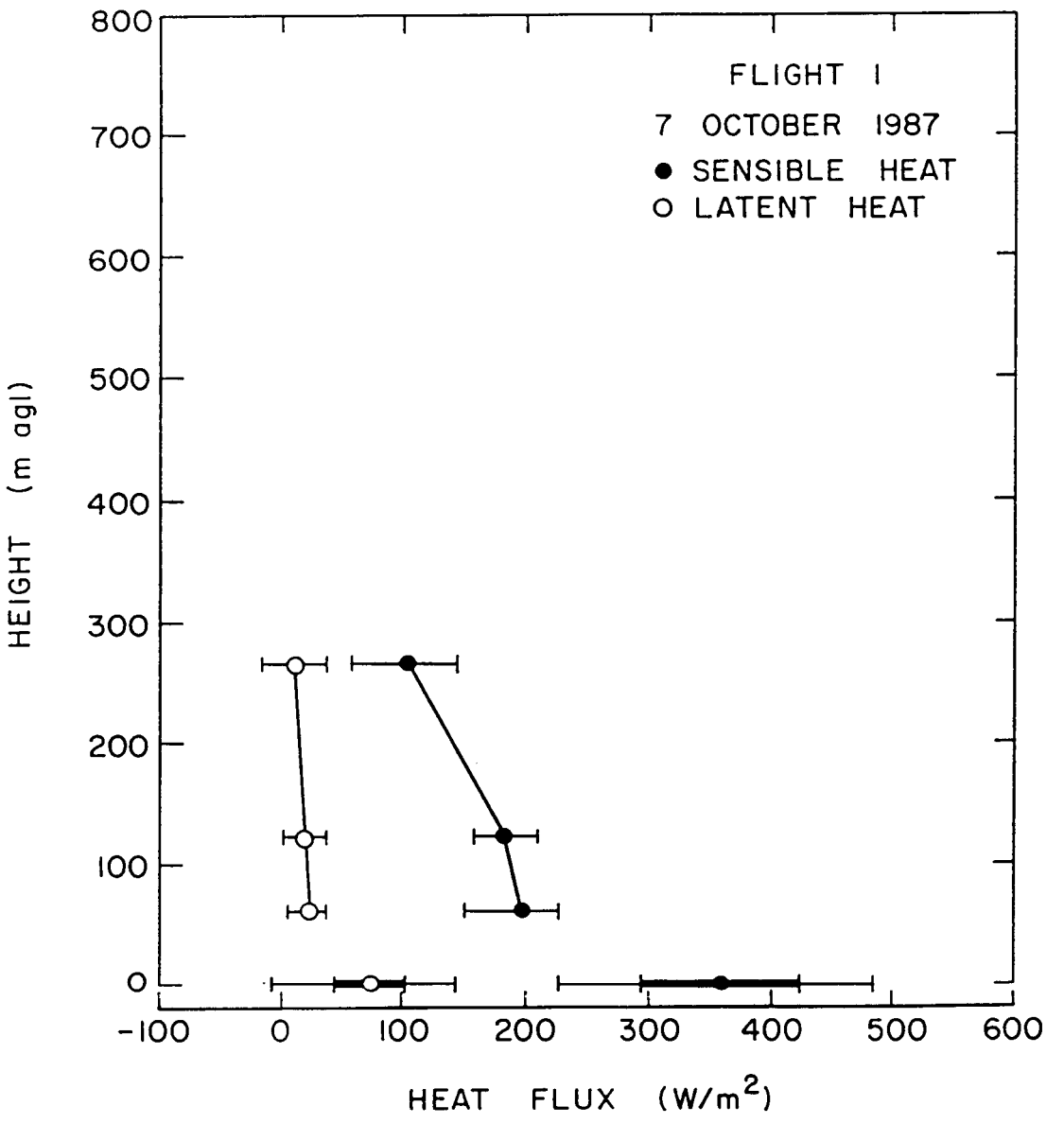

Fig. 8. Same as Fig. 4, for first of two flights on 7 October 1987.

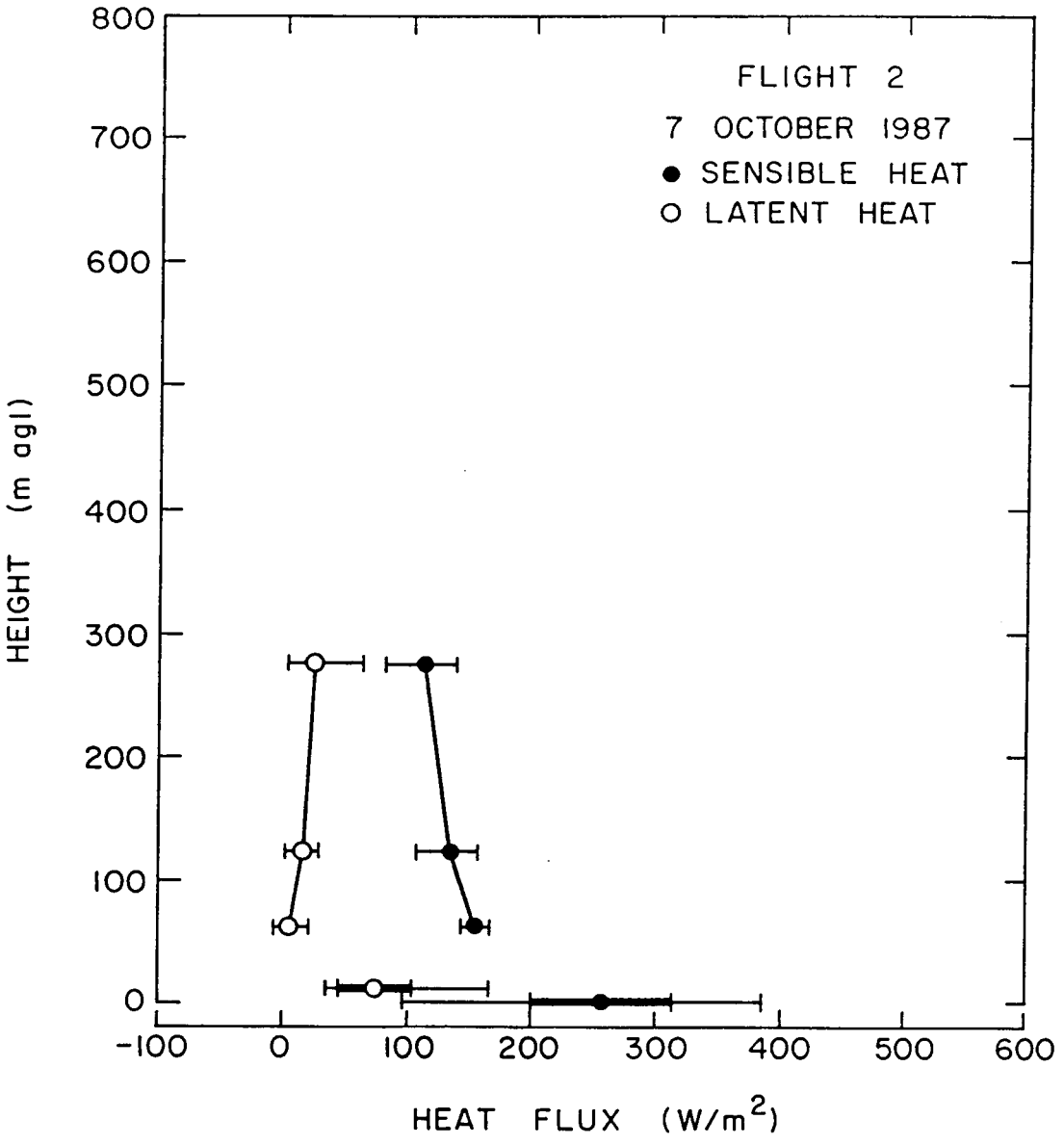

Fig. 9. Same as Fig. 4, for second of two flights on 7 October 1987.

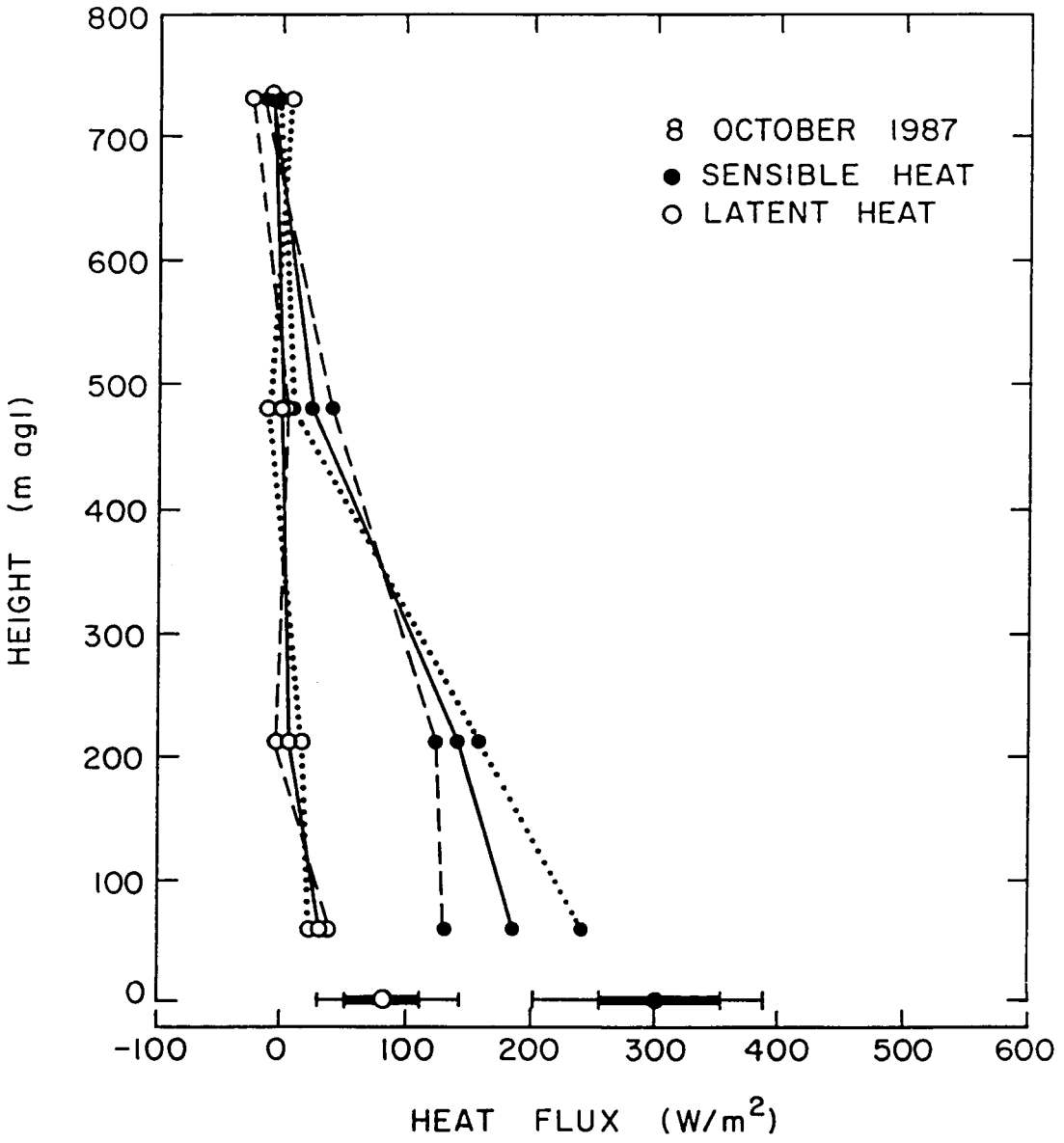

Fig. 10. Same as Fig. 4, for 8 October 1987. The dashed line profile applies to the south end of the FIFE site (FW6-FE6); the dotted line applies to the north end (FNW-FNE); and the solid line is an average of all the measurements for this flight.

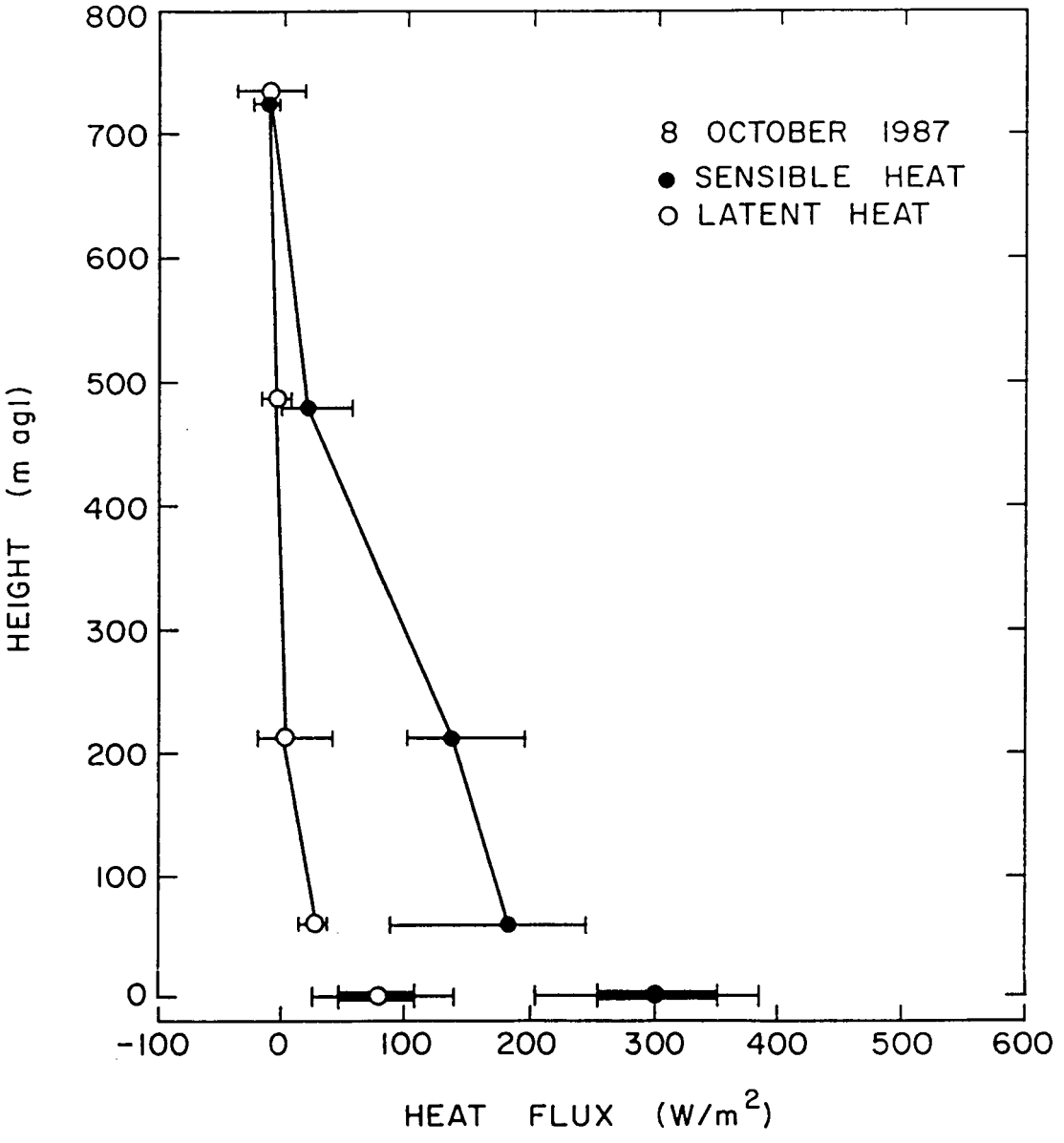

Fig. 11. Same as Fig. 4, for an average of all the measurements on 8 October 1987 (corresponds to the solid line profile of FIg. 10).

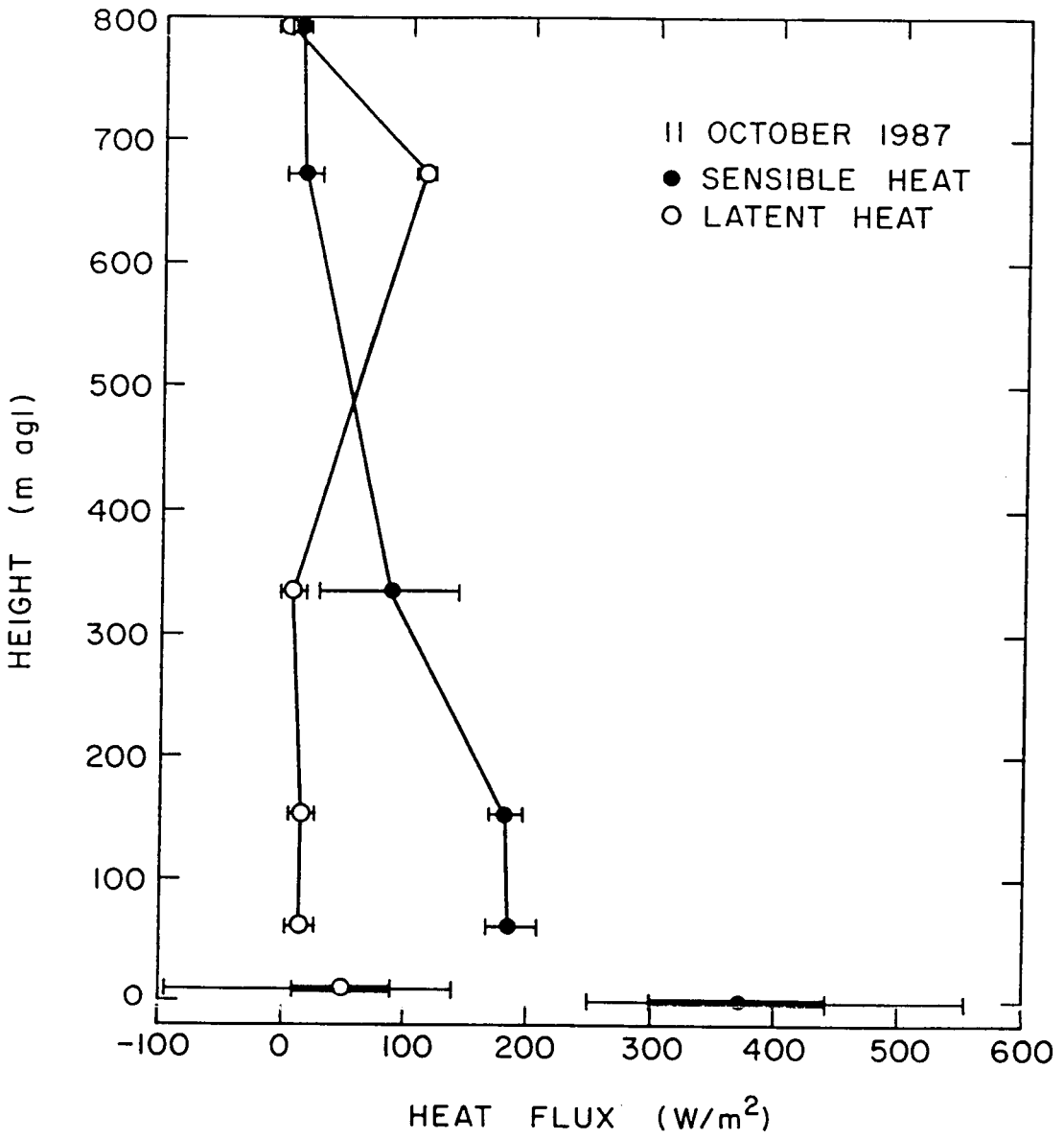

Fig. 12. Same as Fig. 4, for 11 October 1987.

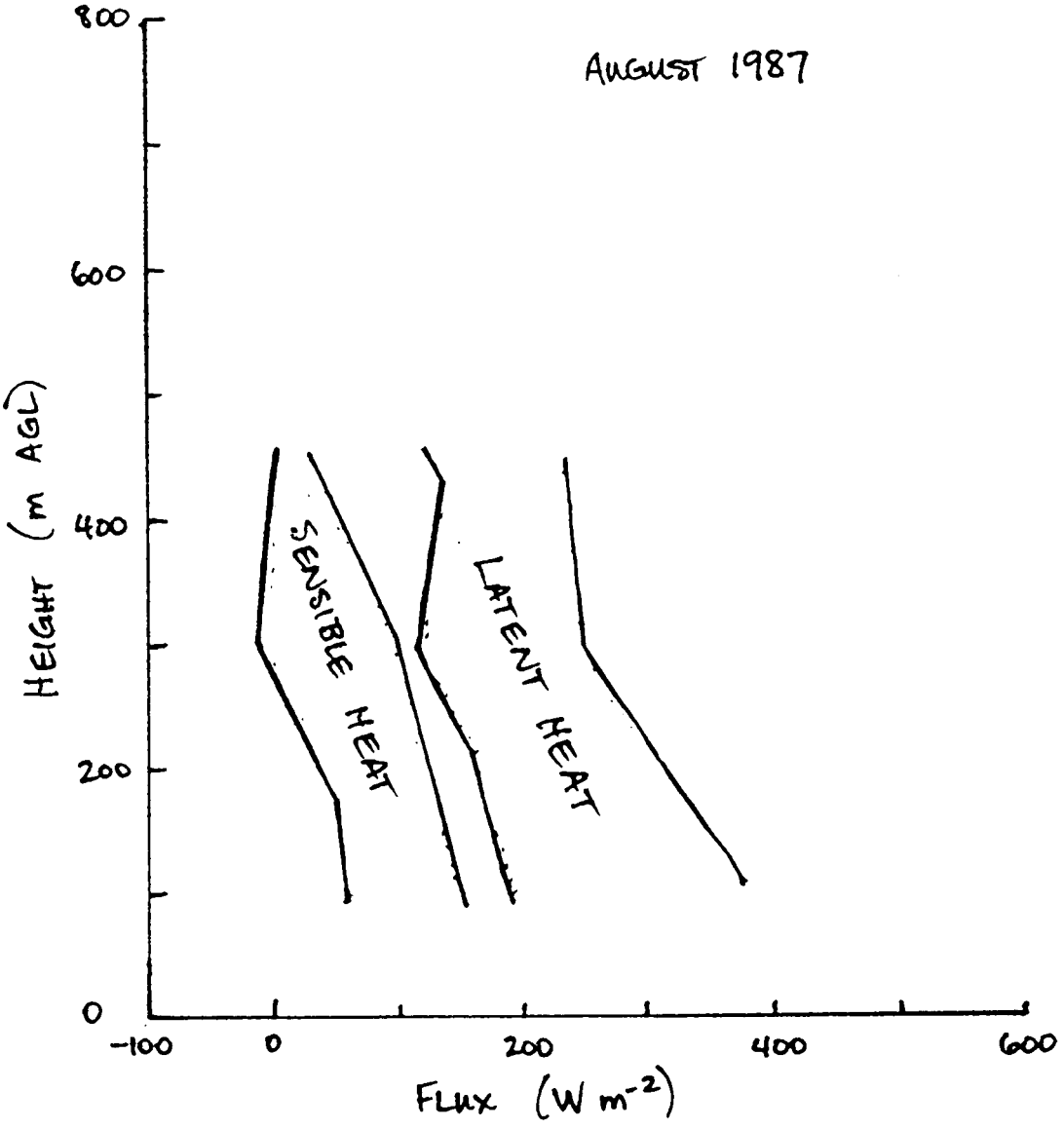

Fig. 13. Ranges of values for all the sensible and latent heat flux profiles measured in August 1987 (August 11, 15, 17, and 20).

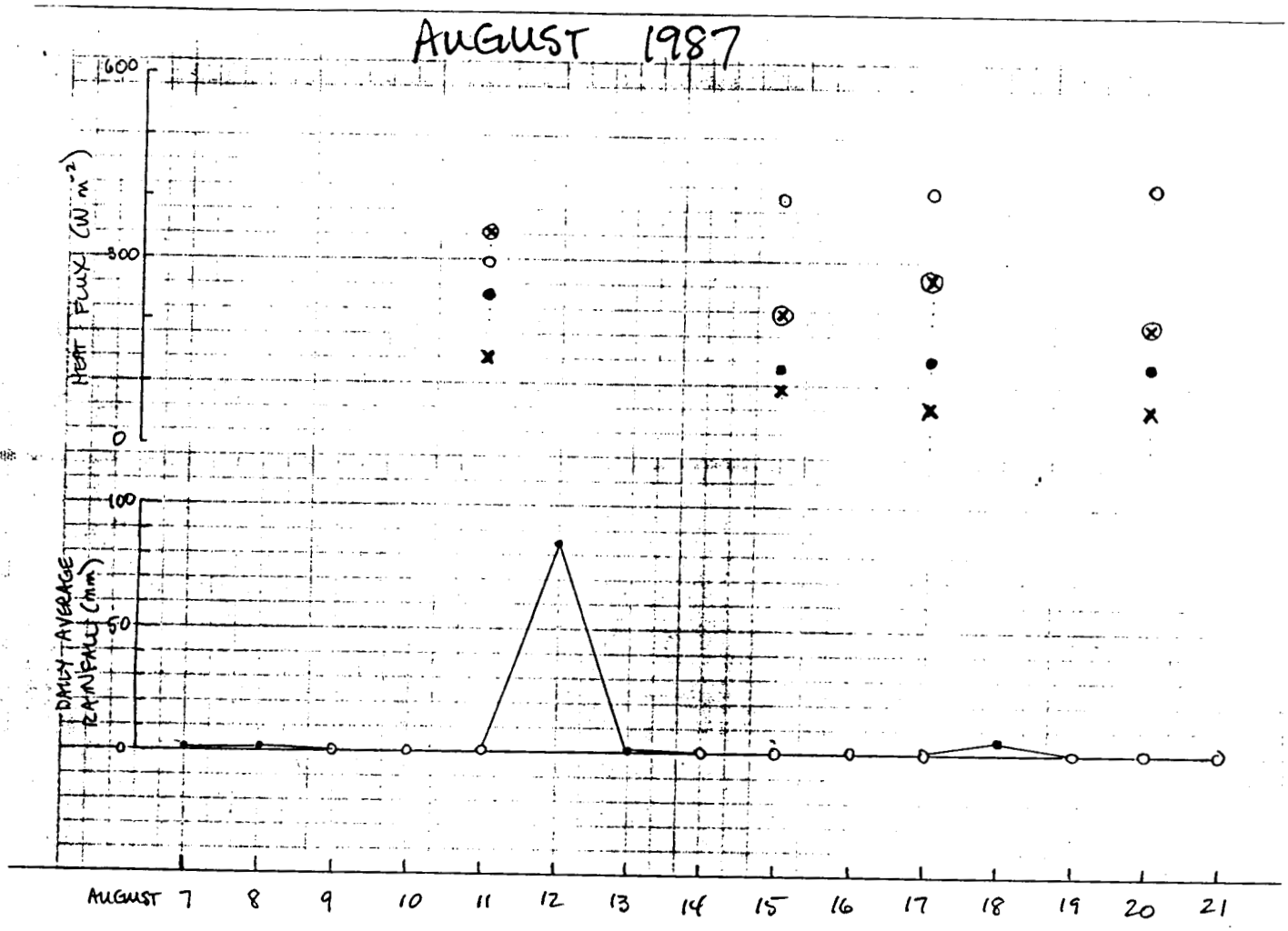

surface: ● sensible heat flux } average of all stations
○ latent heat flux }

aircraft (lowest level in profile):
× sensible heat flux
⊗ latent heat flux

Fig. 14. Time series of flux values and daily average precipitation for August 1987. The flux values are from the Wyoming King Air and from the surface stations (see figure for symbols).

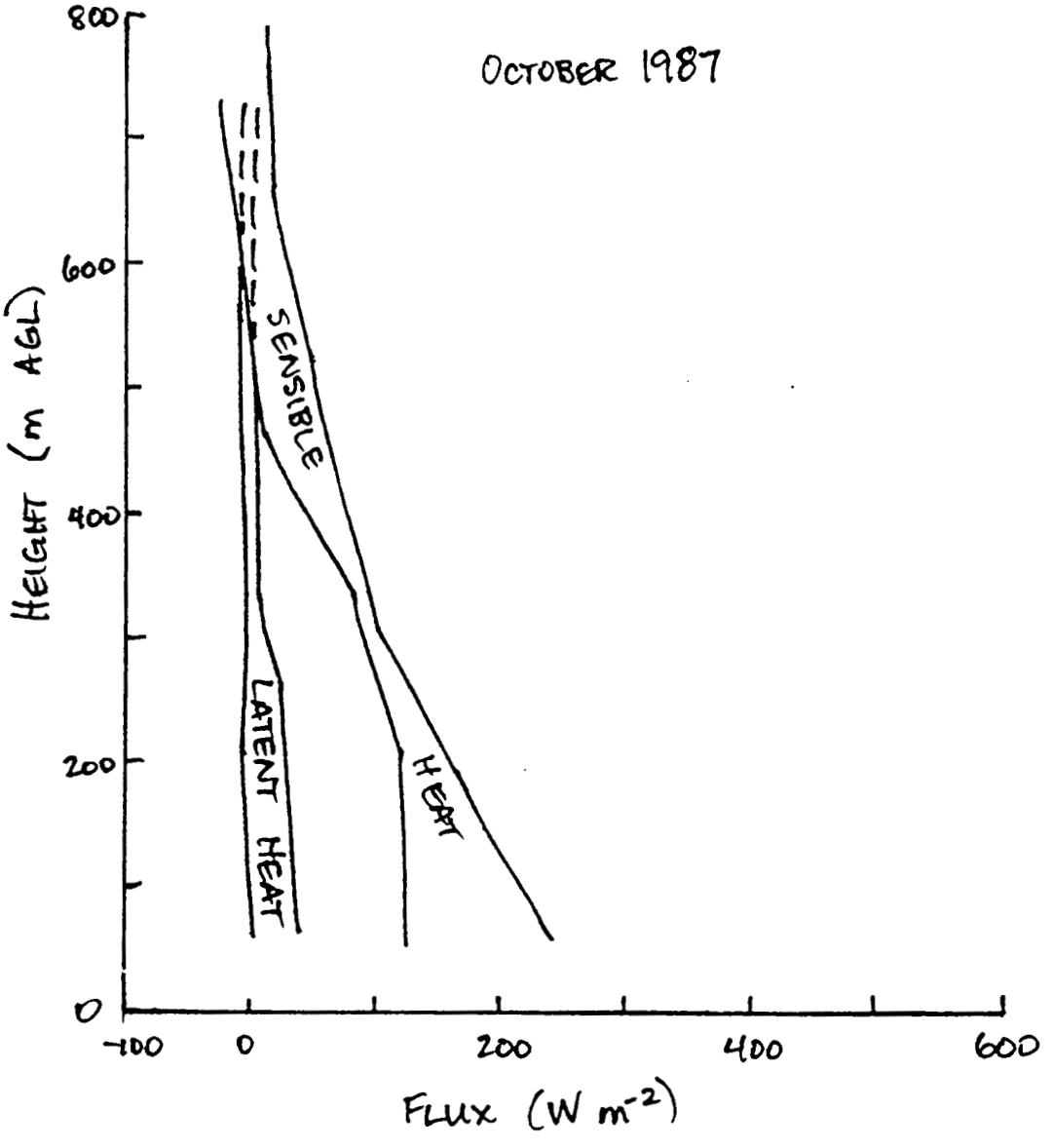

Fig. 15. Same as Fig. 13, for October 1987.

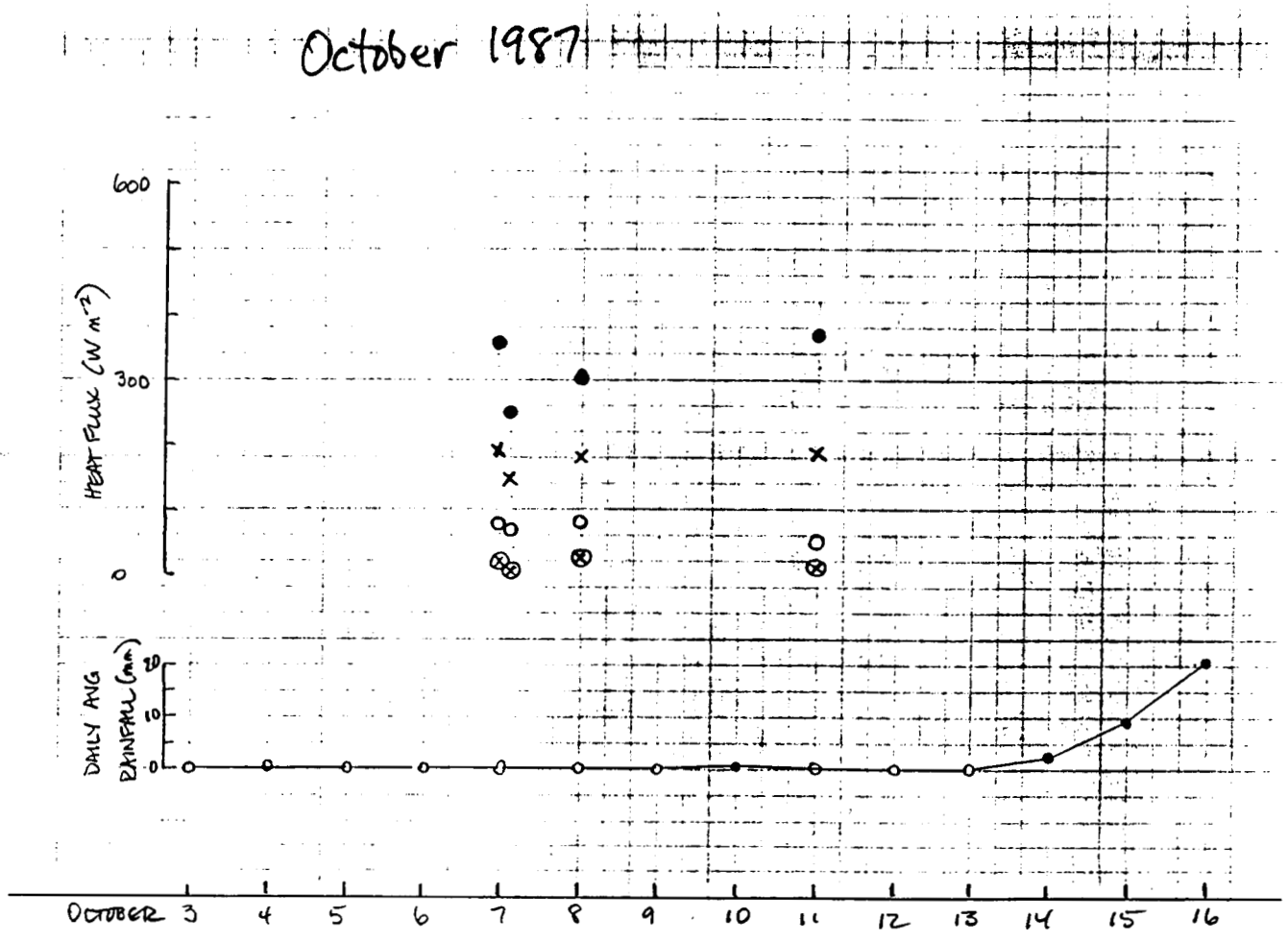

Fig. 16. Same as Fig. 14, for October 1987.

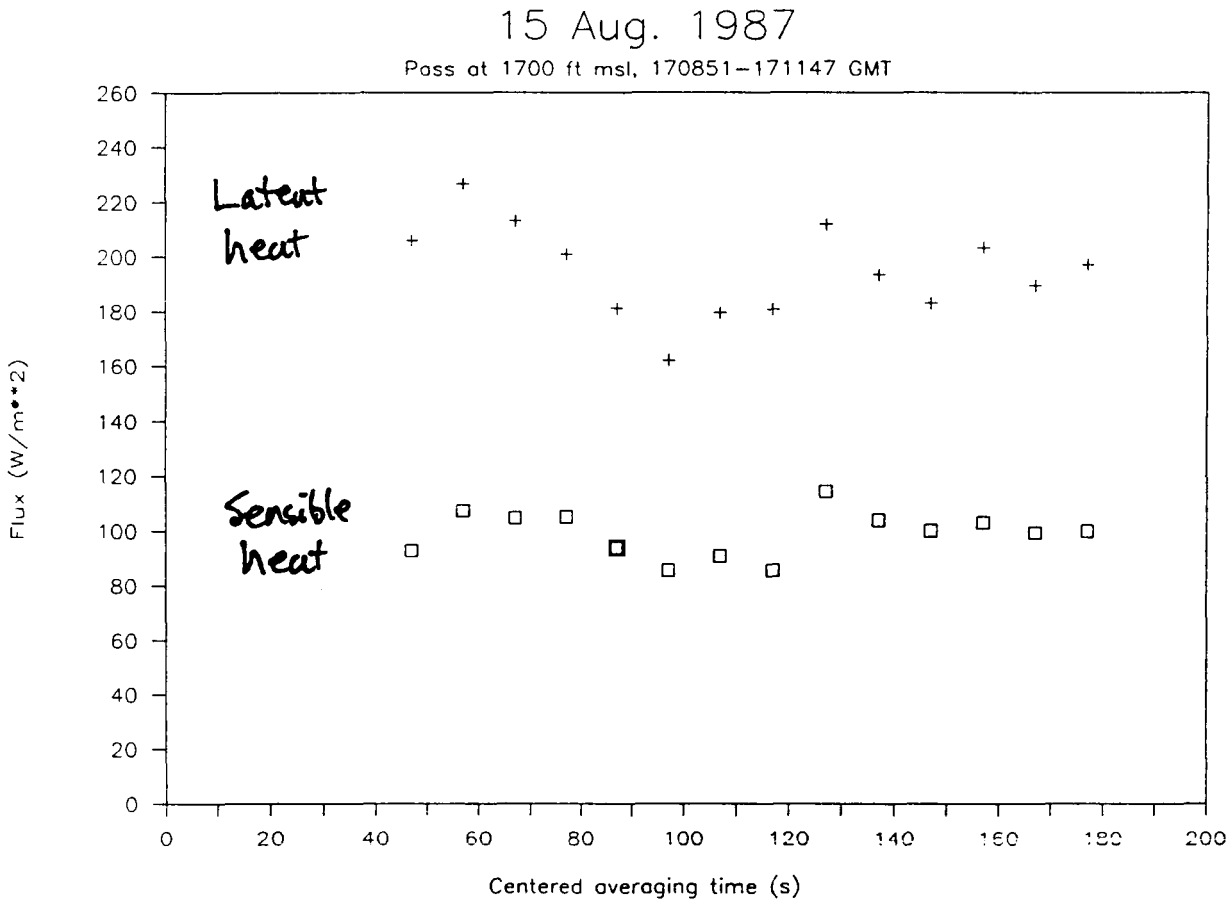

Fig. 17. Pass-average aircraft-measured fluxes as a function of the length of the flight path used for the calculations, i.e., as a function of the length of the averaging period, for time periods all centered at the mid-point of the longest period. The data are for 170851-171147, 15 August 1987, at 1700 ft msl.

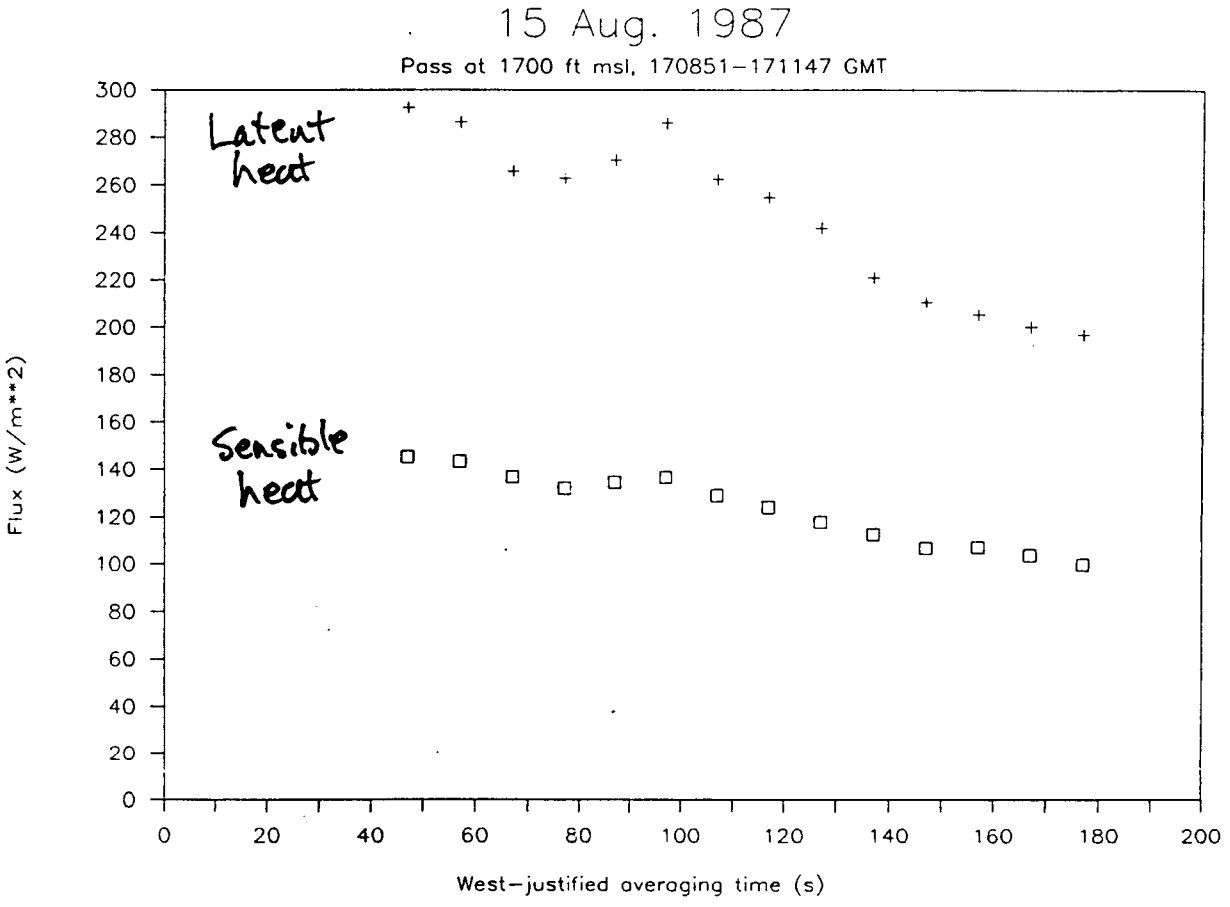

Fig. 18. Same as Fig. 17, except all the averaging periods start at the same point as the longest period (the west end-point of the aircraft pass).

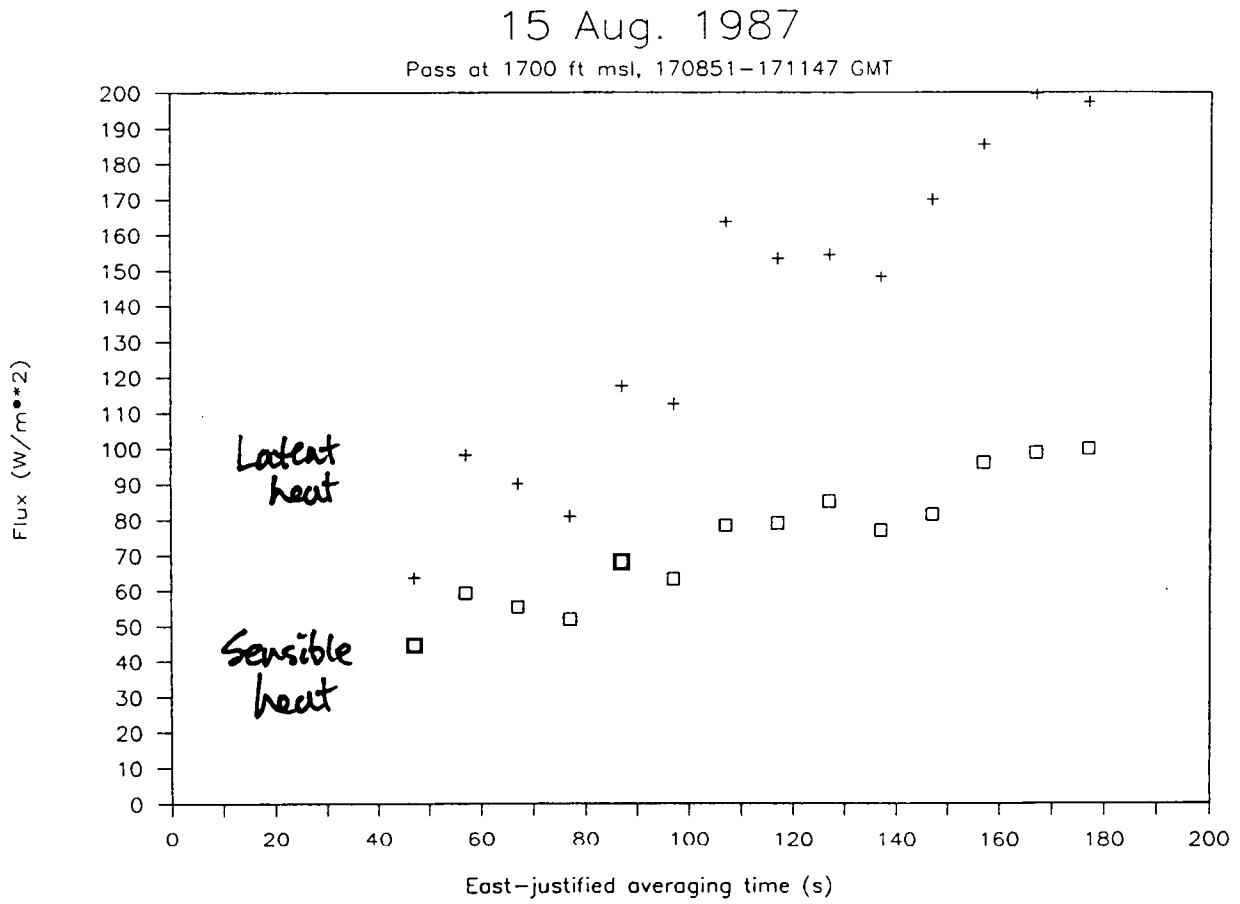

Fig. 19. Same as Fig. 17, except all the averaging periods end at the same point as the longest period (the east end-point of the aircraft pass).

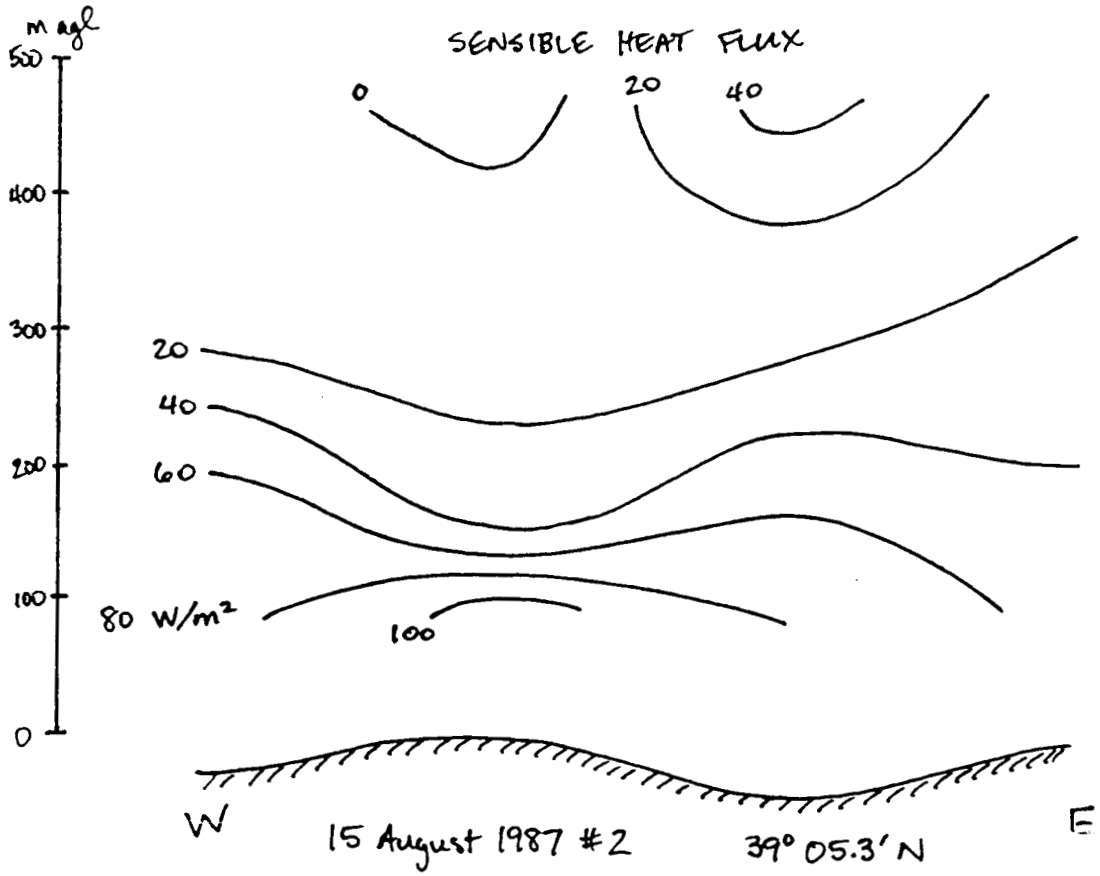

Fig. 21. Same as Fig. 20, for profile 2 on 15 August 1987.

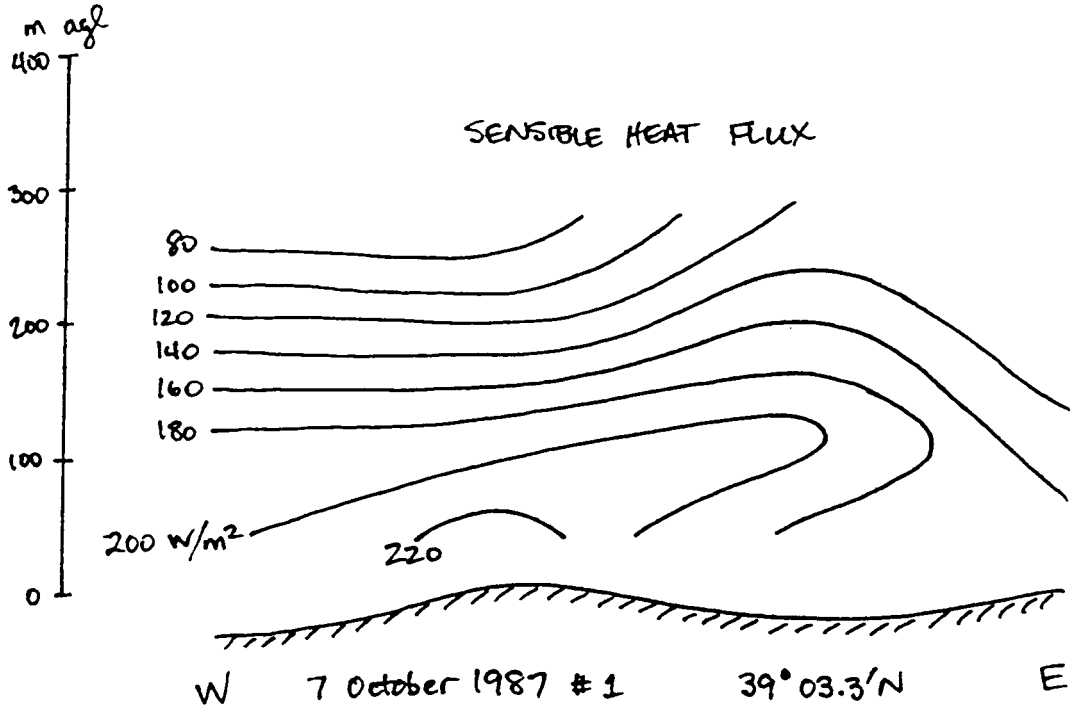

Fig. 22. Same as Fig. 20, for profile 1 on 7 October 1987.

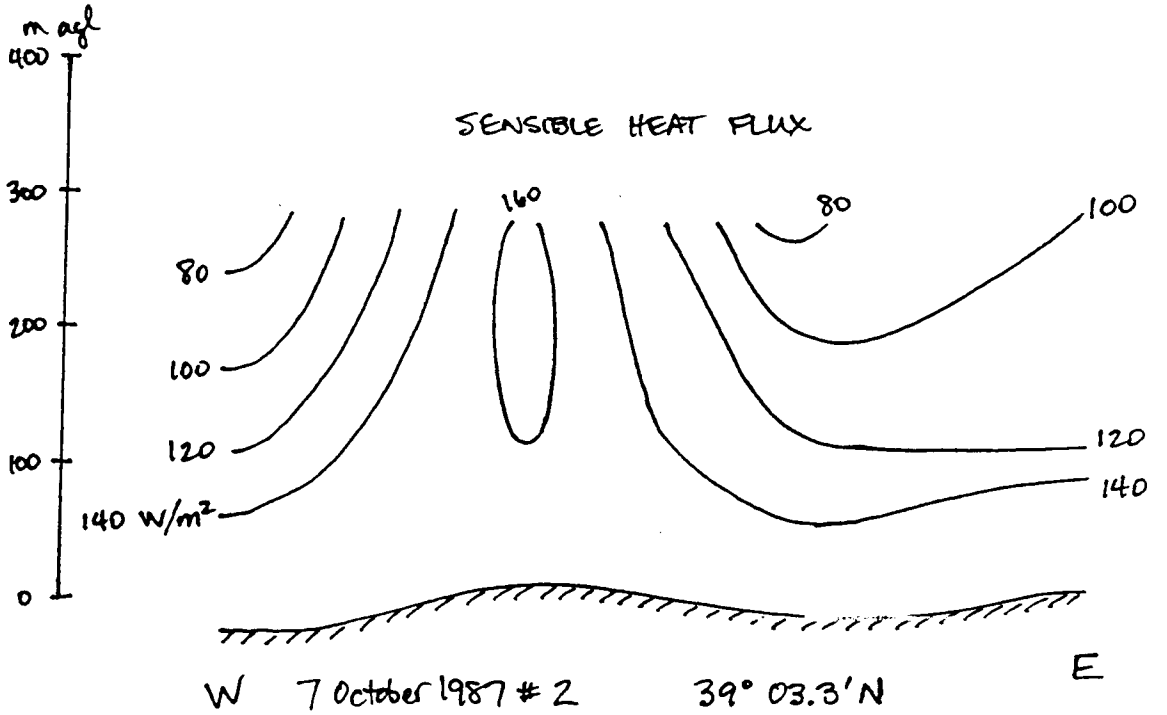

Fig. 23. Same as Fig. 20, for profile 2 on 7 October 1987.

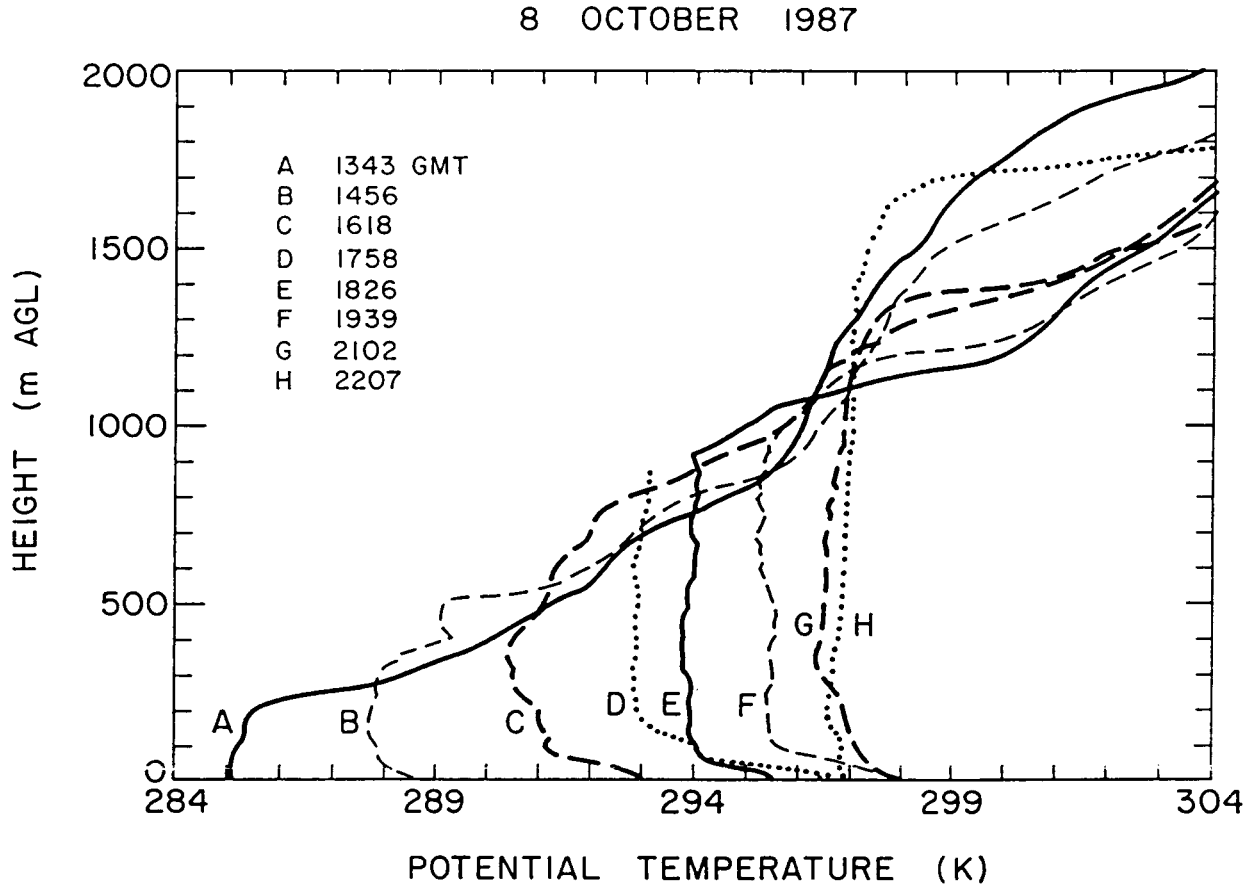

Fig. 24. Sequence of vertical profiles of potential temperature as measured by the FIFE radiosondes on 8 October 1987.

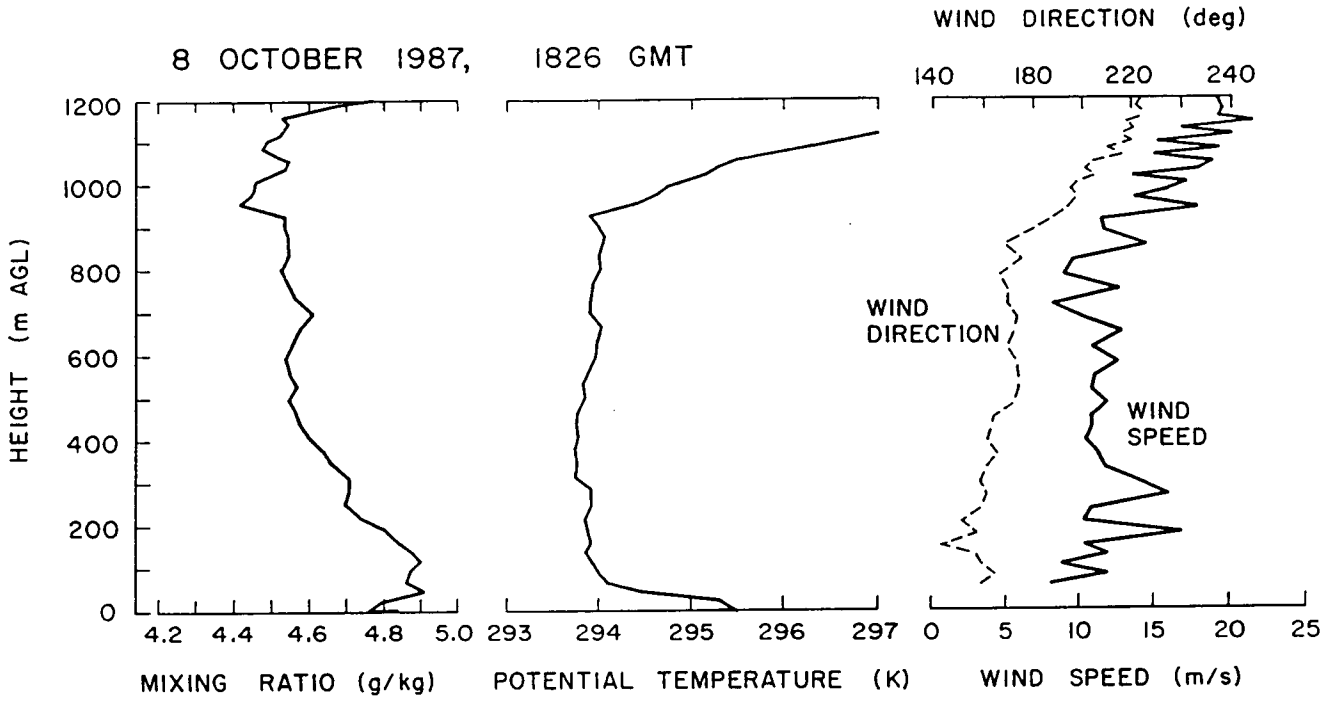

Fig. 25. Vertical profiles of mixing ratio, potential temperature, and wind speed and direction from the FIFE radiosonde released at 1826 GMT, 8 October 1987.

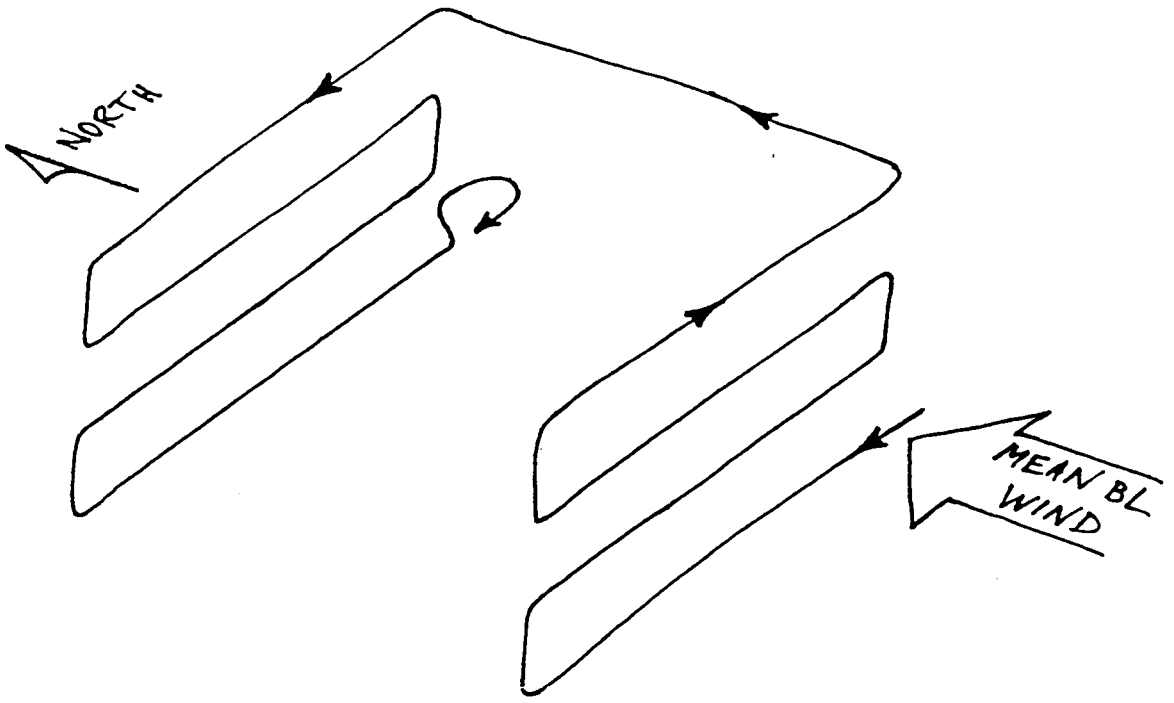

Fig. 26. Three-dimensional schematic of the time-centered flight pattern used in the boundary-layer budget study of 8 October 1987.

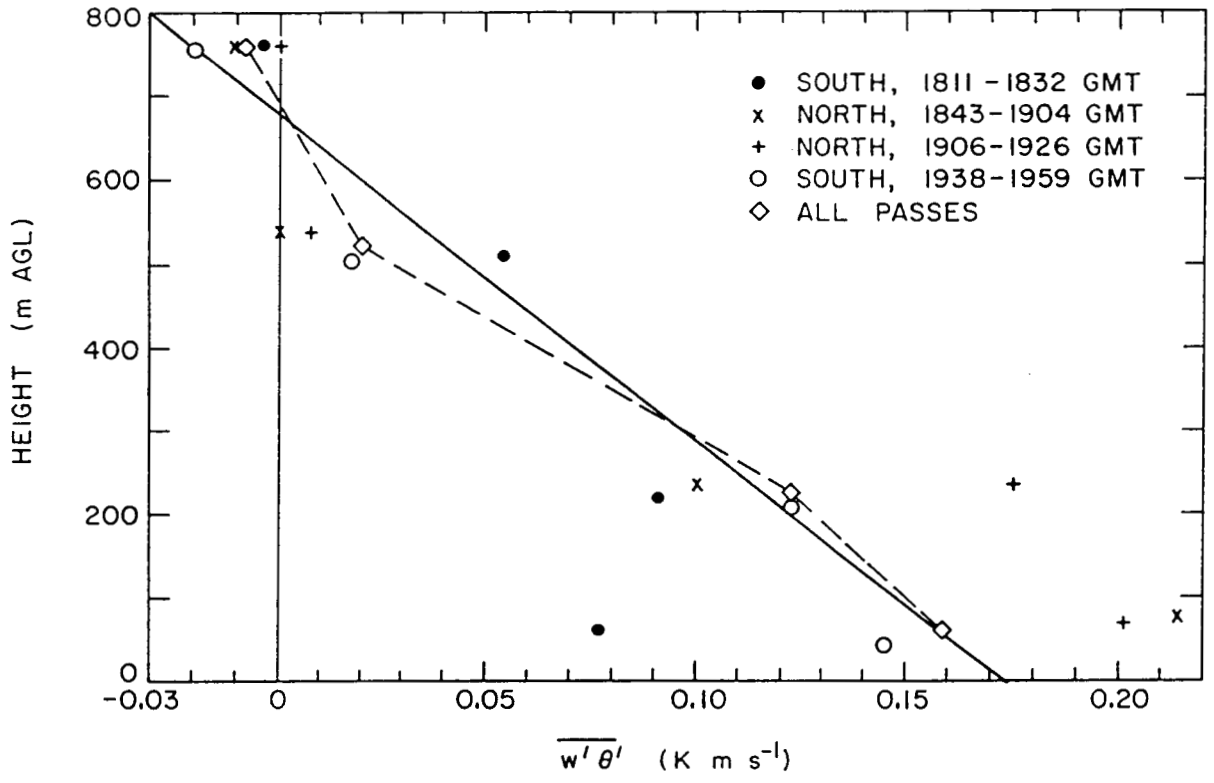

Fig. 27. Vertical profile of pass-average $\overline{w'\theta'}$ for all passes on 8 October 1987. The dashed line connects the level-average values (diamonds). The solid line is the least-squares fit to those same values.